Candidate Performance Summary (Draft)

Ruben Conceição, Jonas Glombitza, Harm Schoorlemmer, Andrew Smith,
for the Analysis and Simulation Working Group

25th March 2024

In this document, we present the performance of the ensemble of designs defined for the M5 milestone. We present here the effective area, hadron-rejection performance and angular resolution of each array layout and unit design. Finally, we conclude by computing the sensitivity curves for each design as a function of energy.

Contents

1 Introduction

As part of the M5 milestone, we defined 13 detector configurations [1], which were devised to be roughly cost-equal. The configurations were chosen to evaluate two independent design choices: 1) The choice of detector unit design and 2) the detector layout, assuming both choices are loosely coupled. In each configuration, there is a trade-off between priorities. For example, a more expensive but possibly superior instrument will cover less area for equal cost and possibly deliver poorer performance. Similarly, configurations that deploy more or fewer detectors in the inner high-density zone will likely see improved or reduced performance at low energy at the cost of high-energy performance. The purpose of this exercise is to evaluate each of the configurations, understanding how the choices made in each configuration improve or worsen the scientific performance of the instrument to serve as input for a detector unit design and layout.

1.1 Detector Stations

We consider 6 detector stations labeled A-F. The designs of these stations explore a space of traditional and novel designs as described in the M5 document. For clarity, we describe here the gross features of each detector and the benefits. Figure 1 shows the 6 detector stations designs considered. The detector station designs can be divided into 3 general types:

1. Double Layer - A,B,C,D - 2 optically isolated cells. The top cell serves as an EM particle detector and the bottom for muon detection.
2. Mercedes - E - A novel design utilizing 3 PMTs in a single relatively shallow layer with white walls.
3. Single Layer - F - A one cell design with PMTs mounted at nearly 4m below the water surface. This design is very similar to both HAWC and LHAASO.

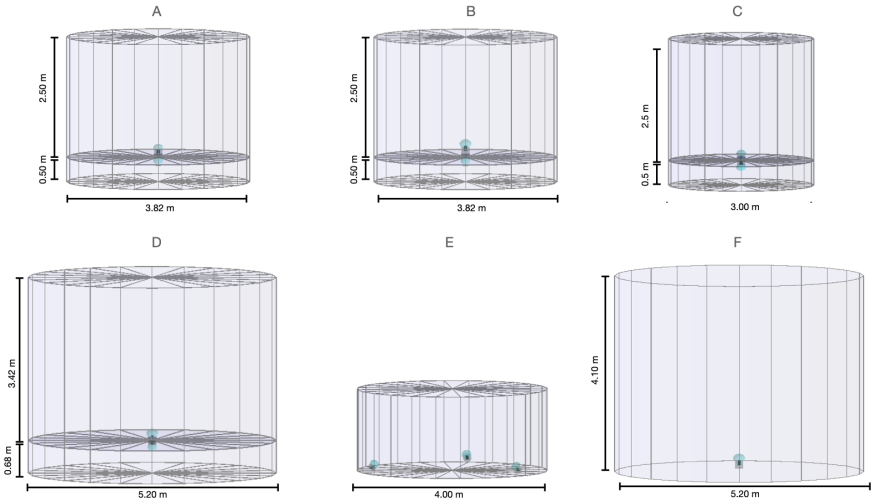

Fig. 1 Unit Designs.

1.1.1 Station Design Motivation

Each of the station designs was considered as a tool to understand performance trade-offs. The motivation for eac design is as follows

- **A** - The A-tank design closely resembles an early SWGO design [2] studied in detail by Samridha Kunwar, which augments the HAWC/LHAASO deep single-layer detector with a lower cell capable of detecting penetrating muons. The lower cell has white walls to maximize light collection. The tank is instrumented with a single

upward looking 8" Hamamatsu R5912HQE PMT (HQE denotes High Quantum Efficiency) and a standard efficiency R5912 in the lower cell.

- **B** - The B-tank is nearly the same as the A-tank, only with a 10-inch Hamamatsu R7081 replacing the 8-inch R5912 in the upper cell. The larger PMT has 41% greater light collection and this design provide information on the differential benefit a more sensitive photo-sensor.

- **C** - The C-tank is similar to the A-tank, but with a 3.0m diameter instead of 3.82m. Each tank is 40% smaller (by area), and is instrumented with a standard instead of HQE PMT in tank-A, giving it similar light collection per unit area. A smaller tank should exhibit improved timing resolution through finer spacial pixelization, so long as information on this scale is present in the shower.

- **D** - The D-tank is a larger version of the A-tank, with a total area increased by about 1.85$\times$ and an upper cell depth increase of 0.92m, more than 2 radiation lengths. The PMT sizes have been increased compared to the A-tank (8" to 10") to maintain a similar light collection per unit area. The large size will provide more crude pixelization, which may compromise direction and core resolution, but this tank has the lowest cost per unit are of the double layer tanks and the increased upper area depth will reduce punch-through making the muon detector more effective.

- **E** - The E-tank (cite articles), or "Mercedes Tank" due to the similarity with the iconic car company's logo when viewed from above, is a novel and innovative design. The design has 3 inward-facing PMTs on the outer perimeter of a relatively shallow tank. Unlike the other tanks, the interior is 100% reflective. The late (reflected) light detected provides an excellent measure of the total deposited light, and the prompt signals from the 3 PMTs identify asymmetries in the shower particle positions. Analysis of the prompt and delayed signals by a NN can provide a novel metric for gamma/hadron detection, different from the penetrating particle detection methods of the other designs. While the tanks are potentially cheaper than that of the taller A-tanks, the savings is approximately offset by the need for 3 PMTs.

- **F** - The F-tank is inspired by the simple single layer designs of HAWC and LHAASO-WCDA. As demonstrated by those experiments, the station design can achieve excellent gamma/hadron separation by offsetting the PMT from the surface by 4.0m of water, about 10 radiation lengths. In such a detector, low-energy electrons and gamma-rays from EM showers interact in the top of the tank producing only small signals in the PMT, but deeply penetrating muons produce large signals. The large size and simplicity of the design makes this tank the least expensive per unit area.

Each station considered explores a different design choice. Our strategy is to compare each station using the A-tank as a baseline. The central questions to be answered by each station design considered in this study are: will be answered by comparing the performance to the A-tank design are:

B) Is a larger PMT beneficial at the cost of fewer detector units?

C) Is a reduced tank size beneficial at the cost of decreased coverage?

D) Is the sensitivity loss due to increased tank size compensated by a larger coverage?

E) Is this novel design, exploiting 3 PMTs in a shallow tank, comparable to or superior to the other designs w.r.t. energy threshold, background rejection, and angle and energy reconstruction?

F) How does the *traditional* design similar to HAWC and LHAASO-WCDA compare to the alternatives? In particular, we will compare the performance with the D-tank as a direct assessment of the benefit of the second layer.

The choice of sizes are were based on known available products at the time of the M5 milestone. The number of stations was based on a fixed totals cost estimated during the same period. Detector stations sizing and pricing is has changed in the intervening period. In particular, the plastic tank designs for the E-tanks, is likely to limit the diameter to 3.6m, while 4-m diameter tanks are simulated here. [1]

[1] Reducing the diameter of the E station would necessitate scaling other specifications to maintain signal uniformity (reduction in water

Detector stations A,B,C,D and F were simulated with white diffusivity reflective walls (Tyvek) and a black ceiling and floor (black polypropylene). The E stations are simulated with all internal surfaces diffusely reflective, since extended photon detection is integral to their novel gamma/hadron separation method. Within the simulation code, we count the number of Tyvek reflections for each photon, so we can, using the same simulated showers, remove or attenuate the late light from the white walls by introducing an efficiency for detection based on the number of reflections to approximate an all black tank. This way, we can compare the performance of all-black vs walls-white tanks.

A summary of the detector considered detector stations evaluated in this study can be found in table 1.

Label	Layers	PMT (upper + lower)	Diameter (m)	Depth (m) (upper)	Depth (m) (lower)	Nominal Cost (kUSD)
A	2	8"HQE + 8"	3.82	2.50	0.50	9.68
B	2	10"HQE + 8"	3.82	2.50	0.50	10.66
C	2	8" + 8"*	3.00	2.50	0.5	6.90
D	2	10"HQE + 8"	5.20	3.42	0.68	14.32
E	1	3×8"	4.00	1.70	-	11.82
F	1	10"HQE	5.20	4.20	-	11.54

Tab. 1 Summary of the detector unit designs exploited in the Candidate Configurations proposed for the **M6** study. PMT labels: 8" = Hamamatsu R5912, 8"HQE = Hamamatsu R5912-100, 10"HQE = Hamamatsu R7081-100. 8"* = 3"PMT + Wavelength shifter plate for costing. Currently, we cannot simulate it, so instead, an 8" PMT will be simulated, and a fraction of the photon electrons will be rejected in post-processing.

1.2 Detector Layouts

In addition to the evaluation of the detector station performance, we also wish to understand the optimal detector station layout. Generally, with a fixed number of detector stations to work with, the layout can either be dense, to detect and reconstruct the lowest energy showers with high efficiency, or sparse to maximize the total detector footprint, extending the effective area for the highest energy showers. However, it is not this simple, since there are likely nearby correlations in the shower front, it is not clear that the best detector for the lowest energies is the most compact. Similarly, even for high-energy showers, higher density leads to improved reconstruction (angular resolution and background rejection), so it is likely that below density the high-energy performance will worsen, even though the total collection area grows. Finally, the trade-off may be a scientific one, eg. Pevatrons vs GRBs, which we endeavor to inform. To this end, we simulate a number of graded arrays (dense central zone with sparse outer zone(s). We simulate arrays with physical footprints from $0.28 km^2$ to $4.5 km^2$. We also explore the effect of "clustering" stations in small groups within the sparse array, a configuration which may have a significant cost savings.

The motivation of each layout is as follows:

Layout 1 - Reference Layout. Zone 1 has an 80% coverage, about as high as possible while still permitting movement between tanks for access and cabling. For the A configuration, Zone 1 has a radius of 160m. Zone 2 has a density of 5% and extends to 300m.

Layout 2 - Extended 2-zone. In this layout zone 2 has been expanded from a 300m radius to a 600m radius. To accommodate the 4× increase in area, the density of zone 2 has been reduced from 5% to 2.5% and the size of zone 1 has been reduced. This configuration covers roughly the same area as LHAASO KM2A.

- Is the large outer zone capable of effective reconstruction?
- What is the cost/benefit of expanding zone 2 at the expense of zone1?

Layout 3 - Extended 2-zone with clusters. In this layout, the size and density of the zone is identical to Layout 2, but the stations in zone 2 have been arranged in clusters of 7 tanks. - How does clustering impact reconstruction and sensitivity?

volume of about 20%), which would, however, lie in a modest area reduction within cost uncertainties.

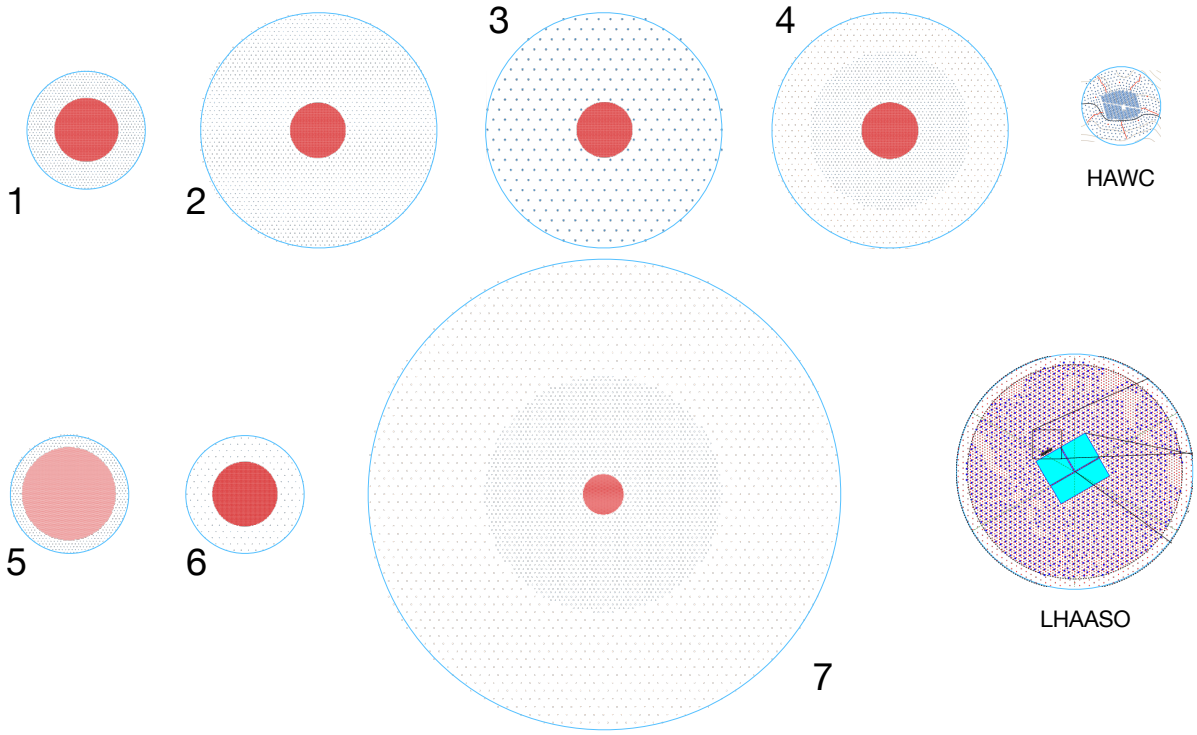

Fig. 2 Configurations 1 to 7 compared to HAWC and LHAASO.

Layout 4 - Extended 3-zone. This layout is a 3-zone array with perhaps better performnce over a range of energies. than the 2-zone layout. We simulated this model for both A and E station designs.
- How does it compare to Layouts 1 and 2, especially for medium to high energies?

Layout 5 - Low-density Core. This layout is similar to layout 1, but has a reduced density in the central zone, 40% instead of 80%. This permits roughly the doubling of size for for the core. The motivation is that shower particles separated only by meters in the shower front may be highly correlated in time and energy, so adjacent tanks will have highly correlated measurements. In this layout we can explore if the expanded area is a greater benefit than the cost of the reduced density.
- Does enlarging the inner array at the expense of a lower fill factor, positively affect the reconstruction and classification of events, particularly in the energy regime around 10 TeV?

Layout 6 - Extreme Density. In this layout, we increase the density of zone 1 to 88%, which is effectively touching, and reduce the density of the zone 2 from 5% to 1%. If coverage at high density is the key to low-energy sensitivity, then this layout may be the best in that energy regime.
- How does this layout compare to layout 1 and 5 at low energies?

Layout 7 - Extreme Size. This 3-zone layout is extremely large, 4.5 km^2 in area. This is achieved with extremely low fill factors and by reducing the size of zone 1.
- How does reducing investment in the inner array impact performance at low energy versus gains at higher energy, and what is the feasibility of incorporating a large low-density zone?

We can create complete configurations by combining a station type (A to F) with an array layout (1 to 7). We denote each simulated configurations with a descriptive label, eg A1 or E4. Since the station sizes vary, the station separation was varied with configuration to achieve the desired fill factor in each zone. Since the total coverage area depends on the choice of stations in our constant costing model, the boundary between zone 1 and zone 2 was adjusted to reduce/increase the station count to match the prescribed value.

We simulated all the station types using layout 1 (A1,B1,C1,D1,E1,F1) to fairly compare station types, and we

simulated all 7 layouts with station A (A1,A2,A3,A4,A5,A6,A7) to compare the layout schemes while holding the detector type constant. We also simulated the E station with layout 4 (E4), since its unique gamma/hadron separation methodology may yield benefits for an large detector.

A summary of the candidate array configurations is presented in Table 2.

Config.	Zone 1			Zone 2			Zone 3		
	FF(%)	Radius (m)	Units	FF(%)	Radius (m)	Units	FF(%)	Radius (m)	Units
A1	80	160	5731	5	300	858			
B1	80	131	3865	5	300	984			
C1	80	137	6829	5	300	1542			
D1	80	166	3367	5	300	438			
E1	80	150	4639	5	300	822			
F1	80	188	4303	5	300	378			
A2	80	138	4303	2.5	600	2328			
A3	80	138	4303	2.5*	600	2520			
A4	80	140	4429	4.0	400	1518	1.25	600	678
A5	40	234	6109	5.0	300	432			
A6	88	162	6469	1.0	300	168			
A7	80	101	2335	2.5	600	2394	0.63	1200	1842
E4	80	140	3403	4.0	400	1428	1.25	600	624

Tab. 2 Summary of the configurations evaluated in the **M6** exercise.

2 Summary of Simulation & Reconstruction

The details of the simulation and reconstruction framework employed to derive the instrument response functions (IRFs) for the candidate configurations discussed in this document are outlined in [3] (SWGO R&D phase plane deliverable *D6.1* [4]).

The software chain's general overview is summarized in Table 24. The table is organized by the step of the analysis chain and provides details such as the name of the executable or library used, along with a brief description of each step.

Program/Library	Description	Language
`corsika`	simulates particles showers	fortran
`hawc-sim`	simulate detector response to particles	C++
`swgo-reco`	• Simulates PMT response. • Reconstructs air shower properties. • Outputs: event level parameters, charges and times, muon-tagging info, mc-true values.	C++
`pyswgo-make-event-level`	• Reduces output of swgo-reco to only event level parameters. • Adds variables (including "analysis bin")	python
`pyswgo-classify-events`	• Add single variable for GH • Generates cut values for IRFs	python
`pyswgo-make-irfs`	Generates from event lists and selection criteria instrument response functions.	python
`gammapy`	Simulate and study science benchmarks.	python

Fig. 3 Overview of the developed software chain.

2.1 Status of the framework

This document is currently representing the status of the working group progress towards reaching M6. For `swgo-reco` the tag `M6_pass3` has been used. For `pyswgo-make-event-level` and `pyswgo-classify-events` the tag `M6_pass3_v5` has been used. The configuration files and production scripts can be found under the production tags in a gitlab repository [2]. These versions are not yet the final versions which limits the conclusions that can be drawn from the results presented in this document. The limitations of the results presented here are:

- Noise hits have not been simulated per event. We won't be able to do this before M6.
- The direction fitting has not been tuned for all configurations.[3]

3 Employed terminology and definitions

3.1 Event Binning

Events are binned to group similar events for classification in quality and *gammaness*. The binning is based on the reconstructed core location, the zenith angle of the events, and the reconstructed gamma-ray energy. Each array configuration has different regions with detector unit densities, which we refer to as 'zones'. The reconstructed core locations of events are binned by their zone. For the zenith angle, two bins are used, between 0°-30° (from the zenith) and 30°-45°. We use logarithmic bins in reconstructed energy, $\log_{10}(E_{\mathrm{rec}}/\mathrm{GeV})$, with a width of 0.5 ranging from 1.5 to 5.5.

3.2 Array Trigger

Noise hits of different sources will influence the observations. For the M6 milestone we were not able to add noise to each event and perform reconstruction in the presence of noise. However, noise hits will significantly influence the data rate the observatory produces and will be different for layouts and detector designs. A threshold on event properties is, in order to simulate an array trigger[4]. Among all setups we assume the same readout strategy and pick an array trigger threshold that equalizes the observatory data rate at 2.0 GiB s^{-1}. For each event the maximum tank-multiplicity (M_{128}) within a 128 ns sliding window is calculated. In order to contribute to the multiplicity an amplitude threshold needs the be crossed at the detector unit level, for the A,B,C,D,F design this amplitude corresponds to 85% of the single p.e. distribution, while for E it is set to 30% of that distribution. The average $\langle M_{128} \rangle$ and the array data threshold $T = M_{128}$@2.0 GiB s^{-1} is estimated for an array is estimated with waveform simulation that includes the cosmic ray flux,after-pulsing, electronic noise, and dark counts. We estimate the M_{128} at event level[5] for each event, and in we accept it when $M_{128} > T - \langle M_{128} \rangle$. The values for the different setups are shown in table 3.

Note that the 2.0 GiB s^{-1} array trigger was imposed to provide a constant data rate for the detector for each configuration. This approach is taken so that all the configurations have the same DAQ processing requirements and cost. However, this approach potentially has a significant effect on the low-energy sensitivity, since the trigger is not optimized for each configuration independently. The best approach would be to optimize the trigger for each configuration, then add the cost related to the higher capacity DAQ, where needed, to the array costs in our constant cost comparison scheme, reducing the number of active stations to account for increased DAQ costs. This approach is particularly important for the type E tanks, which have 3 PMTs per station and have a fully reflective interior, producing many times the hit rate of the other station designs. To mitigate this effect, for

[2] https://gitlab.com/swgo-collaboration/simulation/classify-events

[3] Some minor tweaks have been performed to improved the performance of the E detector units to get comparable results to other designs.

[4] https://www.swgo.org/SWGOWiki/lib/exe/fetch.php?media=simulations:electronics_and_trigger_simulation.pdf

[5] slide 4-6: https://www.swgo.org/SWGOWiki/lib/exe/fetch.php?media=simulations:20240315_muontaggerupdatesandarraytrigger.pdf

the E-tank comparison, we consider 2 different triggering schemes: 1) The constant data rate scheme presented here and 2) Fixing the trigger at 25 hit stations. The former underestimates the low-energy performance of the E-tank configurations and the latter likely overestimates the performance, but together, they should form a reasonable confidence interval.

Configuration	Threshold T	Average $\langle M_{128} \rangle$
A1	51	26
A2	43	26
A3	44	26
A4	46	27
A5	59	29
A6	52	25
A7	36	26
B1	41	22
C1	57	25
D1	42	23
E1	286	57
E4	283	59
F1	49	22

Tab. 3 Array trigger settings with variables as explained in the text.

3.3 Event Selection

We further apply a cut on the likelihood quality of the template-based reconstruction $\mathcal{L}_{E,\sigma} < 2.1$ and select only events with good angular reconstruction $A_\sigma < 1.8$ to ensure a good and reliable reconstruction. In both cases, events are discarded that are reconstructed with a goodness $\times\sigma$ away from the median of reconstructed events, where σ denotes the standard deviation.

3.4 Effective Area

The effective area characterizes the detection efficiency of a particular instrument or detector system for incident particles. We use the following definition to connect between the simulated quantity of shower events and the quantity of simulated events that trigger the instrument and can be reconstructed, satisfying all selection criteria: The effective area (A_{eff}) for observing a source that transits between θ_{low} and θ_{up} is estimated as:

$$A_{\text{eff}} = \frac{1}{2\pi\,(\cos(\theta_{\text{low}}) - \cos(\theta_{\text{up}}))} \times \frac{\sum_k \omega_k^E \omega_k^R}{n_{\text{thrown}}\,\mathrm{d}E} \tag{1}$$

where ω^{MC} denotes the energy event weight, ω^{R} the radius weight, n_{thrown} the number of simulated events, and k runs over the selected events, per energy (bin) dE.

3.5 Angular Resolution

The Point Spread Function (PSF) characterizes the instrument's angular resolution and is assumed to be radially symmetric. The angular resolution is defined as the containment radius in angular space, which contains 68% of the reconstructed distribution around a given (true) point source.

3.6 Energy Resolution and Bias

We evaluate the difference in reconstructed energy E_{R} and the true (Monte-Carlo) energy E_{MC} in log-space: $\Delta = \log_{10}(E_{\mathrm{R}}/\mathrm{GeV}) - \log_{10}(E_{\mathrm{MC}}/\mathrm{GeV})$. We define the bias as the median of the Δ distribution. As the Δ distribution is asymmetric, with a longer tail towards the negative side, we defined the energy resolution as half the difference between the 15.9% percentile and the 84.1% percentile of the Δ distribution (instead of using a standard deviation).

3.7 Background Rejection

For assessing the rejection performance of the hadronic background, we examine the background rejection ε_p (false positive rate) as a function of energy for a fixed gamma efficiency (true positive rate) of ε_γ = 80%.

3.8 Sensitivity vs Energy

The overall performance of a candidate detector unit or array layout is done by evaluating the flux sensitivity to a steady point source. We picked a source at a declination of -10°, while the detector is placed at a latitude of 20° south and calculate the sensitivity for 1 year of observations (365.25 transits). The source has a power-law energy spectrum with an index of -2, and a reference flux of 1×10^{-11} $\mathrm{TeV}^{-1}\mathrm{cm}^{-2}\mathrm{s}^{-1}$ at 1 TeV. The sensitivity is shown as a function of the reconstructed energy bin and is defined as the flux level where a 5σ detection with at least 10 photons is achieved. In the case that we reject all simulated proton air showers during our gamma-ray selection, we extrapolate the background rate with a spline function. This method is not ideal and implemented to have a smooth sensitivity curves without "holes". The correct thing would be to run a larger simulation set, which of course is very time consuming.

4 Evaluation of station types A-F

In this section, we compare the performance of the 6 different stations types for Layout 1, configurations **A1,B1,C1,D1,E1,F1**. In each section, we summarize the differences between the configurations and the motivation for the designs of each station type. We provide a standard figure showing a direct comparison of the angular resolution, hadron rejection, effective area and overall sensivitiy for the zenith angle range [0,30^o].

For convenience, we present each configuration on a separate page.

4.1 B1: Reference tanks with larger, 10" PMT

Motivation: We wish to examine the possibility of using a larger upward-facing PMT. A larger PMT could offer greater sensitivity by improving the timing and charge resolution. But, there will be diminishing returns at some point since we can never do better than detecting all the particles.

Evaluation: Compare to reference configuration **A1** to see if increased photon collection is beneficial at the cost of a decreased number of detector units.

Discussion: Below 30 TeV all performance parameters are better on the A1 configuration. The better sensitivity for B1 comes most likely from the background rate extrapolation of the outer array of B1, is evident from the lack of background in the proton efficiency figure.

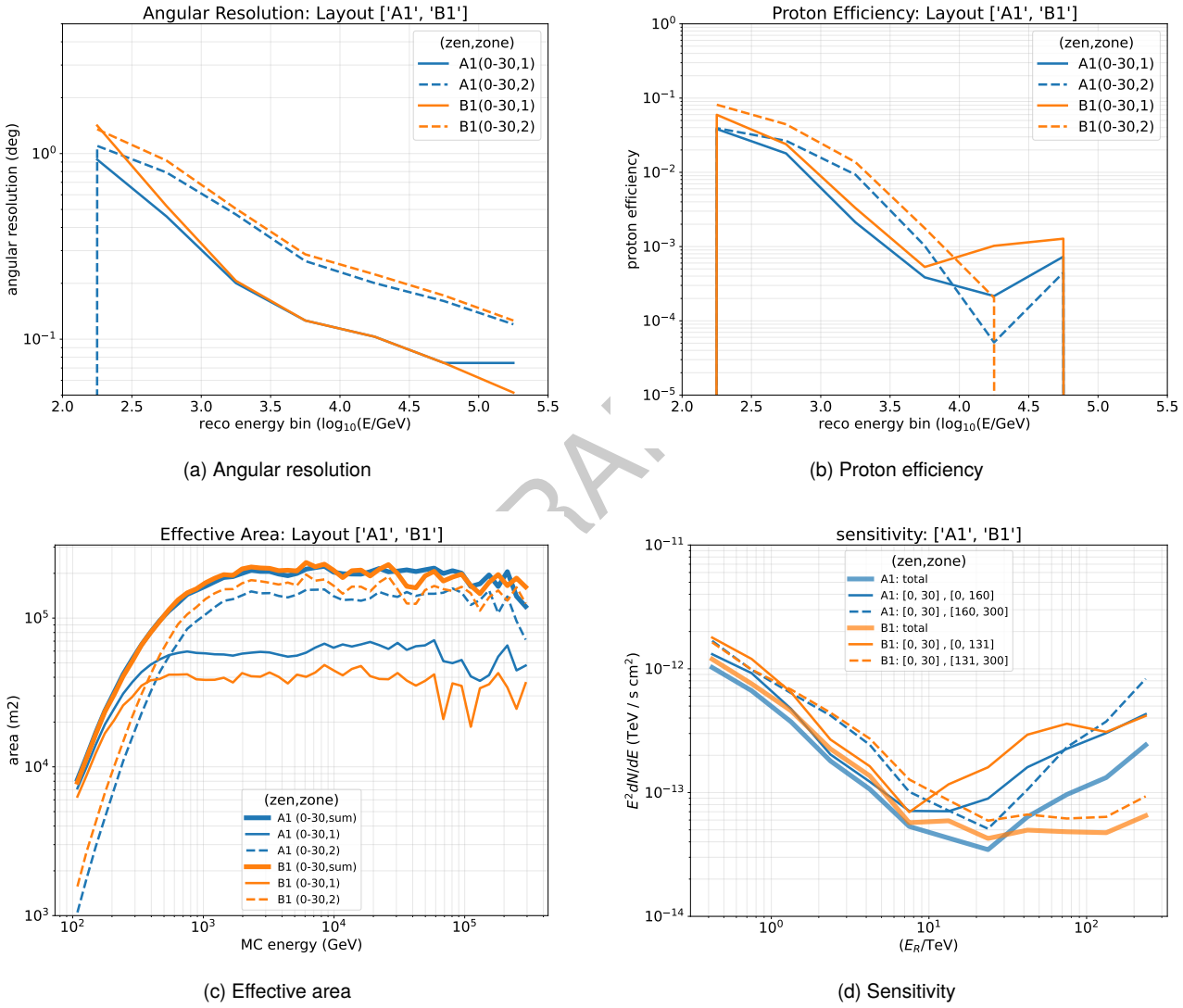

(a) Angular resolution

(b) Proton efficiency

(c) Effective area

(d) Sensitivity

Fig. 4 Angular resolution (a) proton efficiency (b), effective area (c), and sensitivity (d) as a function of the energy of configuration **B1** compared to the reference configuration.

4.2 C1: Reference layout with smaller, 3 m diameter, 2-layer tanks

Motivation: Smaller tanks will permit us to more finely segment the detector. Studies have shown that finely segmented detectors could offer superior timing resolution and better localize the EM energy distribution at the ground, improving angle, core, and energy reconstruction, and possibly also background rejection. Smaller tanks are, however, more expensive (per unit area of coverage) and require additional electronic channels.

Evaluation: Compare to reference configuration **A1** to see if reduced tank size is beneficial at the cost of decreased coverage.

Discussion: The smaller tanks do not show improvement in angular resolution at any energy. Overall, the higher cost per unit area for the smaller tanks leads to a lower effective area and a slightly diminished overall sensitivity at all energies.

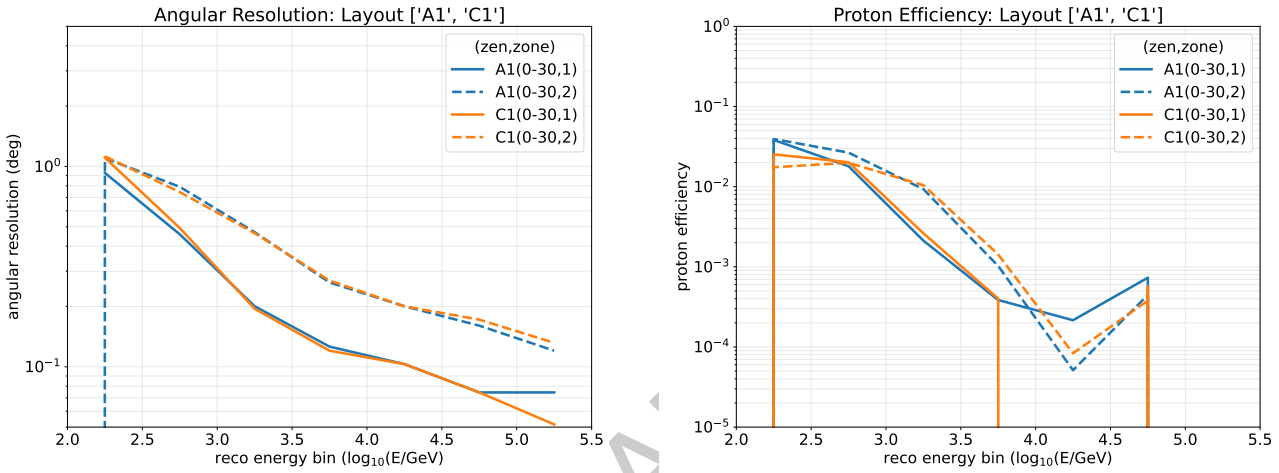

(a) Angular resolution

(b) Proton efficiency

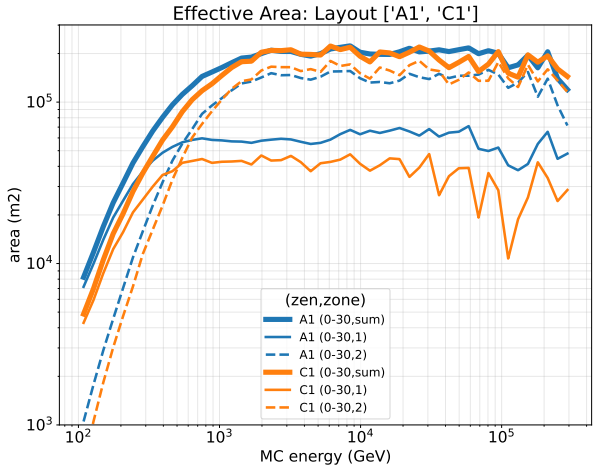

(c) Effective area

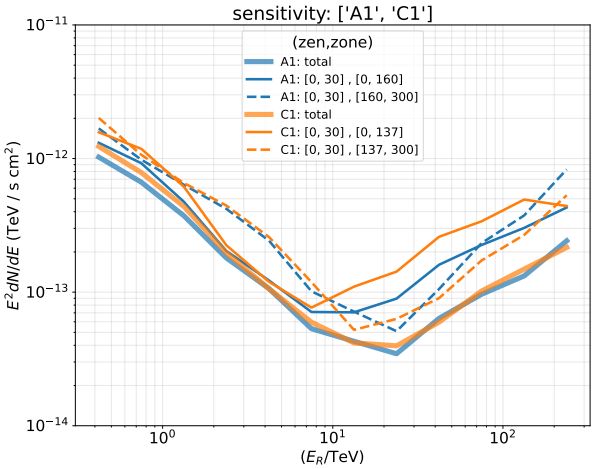

(d) Sensitivity

Fig. 5 Angular resolution (a) proton efficiency (b), effective area (c), and sensitivity (d) as a function of the energy of configuration **C1** compared to the reference configuration.

4.3 D1: Reference layout with larger, 5.2 m diameter, 2-layer tanks

Motivation: We anticipate that larger tanks, though they will likely have poorer angle, core, and energy reconstruction due to the coarser segmentation, may be superior due to their lower cost per unit area of coverage and their deeper upper layer, which provides greater shielding (2 radiation lengths)for the muon detector below, which is likely to improve the gamma/hadron separation.

Evaluation: Compare to reference configuration **A1** to see if the sensitivity loss due to increased tank size is offset by the benefit of a larger coverage.

Discussion: The larger tanks, though showing slightly poorer angular resolution at the lowest energies compared to the A tank, display a much improved hadron rejection capability and greater effective area. The combination of these factors leads to an equal or superior performance compared to A, which improves with rising energy.

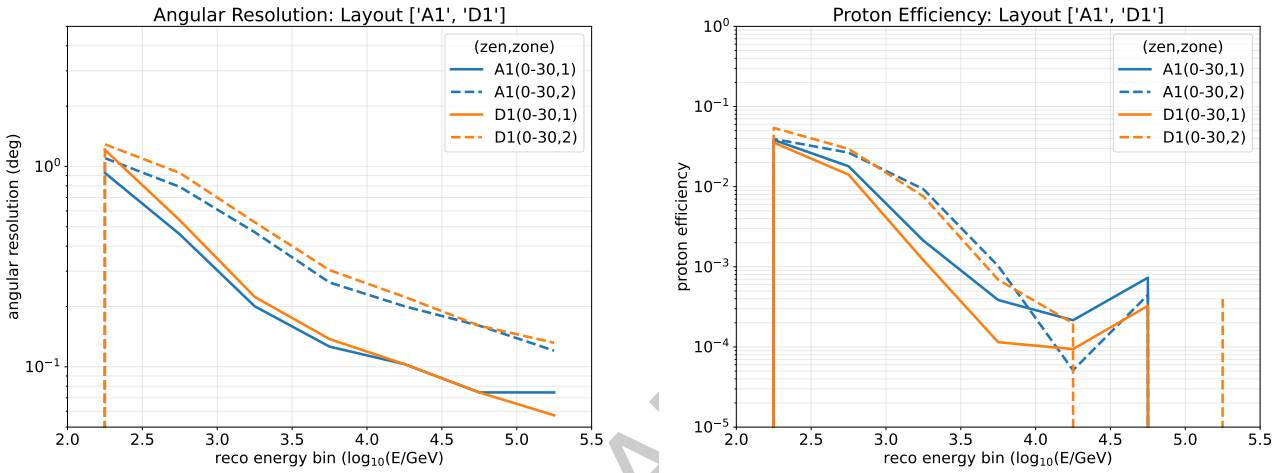

(a) Angular resolution

(b) Proton efficiency

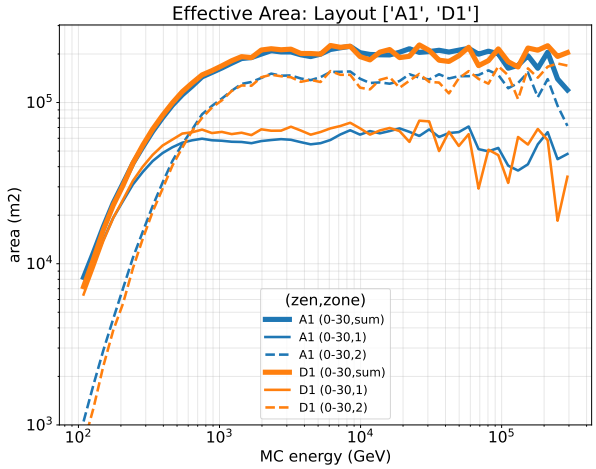

(c) Effective area

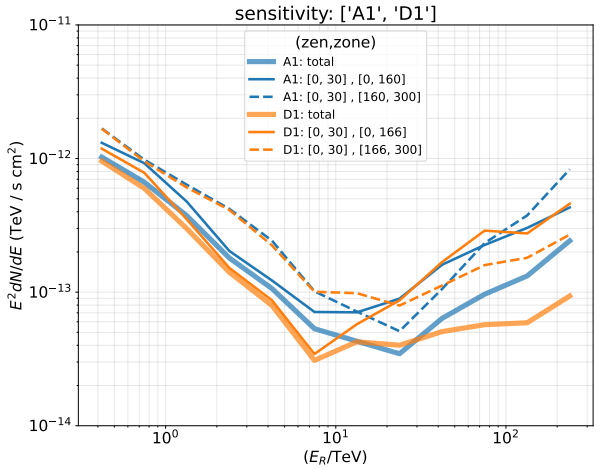

(d) Sensitivity

Fig. 6 Angular resolution (a) proton efficiency (b), effective area (c), and sensitivity (d) as a function of the energy of configuration **D1** compared to the reference configuration.

4.4 E1: Reference layout with Mercedes tanks

Note: The *Mercedes* station (E-tank) is different than the other stations considered here, in that it has 3 PMTs detecting the EM shower directly in each station and it employs completely white interior walls to maximize the delayed light. We find that as much as 2/3 of the detected light is delayed. These two factors increase by nearly an order of magnitude the per-station data rate. As discussed in the previous section, the trigger threshold was defined for each configuration by holding the data rate constant, based on requirements set by the detector group. This approach demands a relatively high trigger threshold for this tank, maybe unrealistically so.

It should also be noted that the very high hit rate in these tanks will also limit the the sensitivity, as it introduces noise that worsens the reconstruction performance. This is not accounted for, as we do not simulate the noise in the reconstruction.

To fully evaluate this station type, we show here two different analyses, one with the uniform data-rate defined trigger and another with an unrealistically low trigger threshold of 25 hits. The former threshold is probably unrealistically high and the latter is unrealistically low.

Motivation: Mercedes tanks, with their novel 3-PMT design, could offer an improvement over the single-PMT-per-chamber approach.

Evaluation: Compare to reference configuration **A1**, paying special attention to each contributing element: threshold, background rejection and angle and energy reconstruction.

4.4.1 Constant data rate array trigger E1 vs A1

Discussion: As described in the introduction, for this comparison, the E-tank shows a significantly lower effective area compared to the A-tank. Note that although the the area is lower by nearly an order of magnitude, the sensitivity at low energy is only slightly worse. This is likely because much, or even most of the low-energy sensitivity comes from events well above the threshold.

The E-tank appears to have slightly superior angular resolution, but seems to have poorer background rejection.

With this constant rate array trigger analysis, the E-tank is not superior to the A-tank at any energy, but similar at medium and high energies, where it is appropriate to compare them.

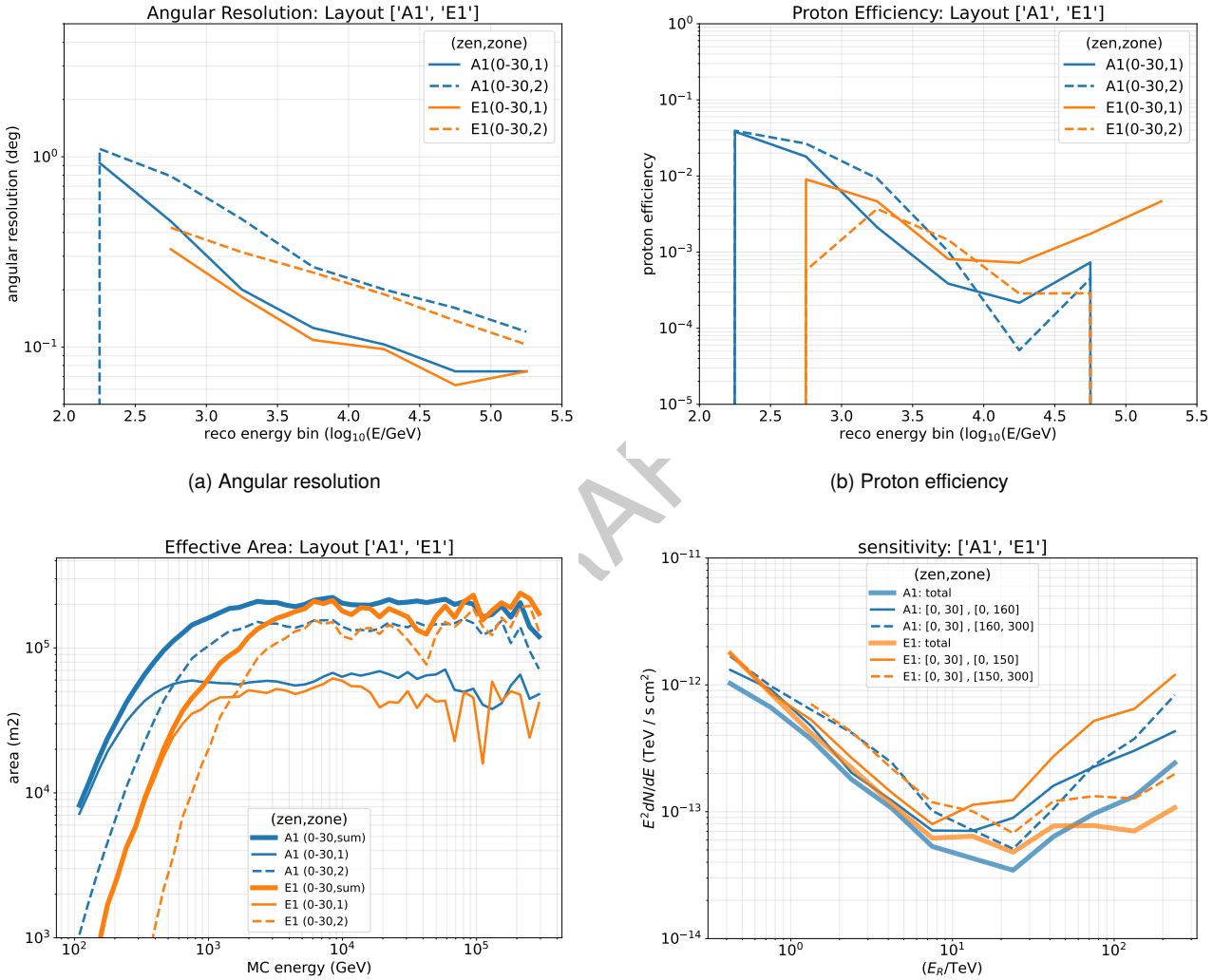

(a) Angular resolution

(b) Proton efficiency

(c) Effective area

(d) Sensitivity

Fig. 7 Angular resolution (a) proton efficiency (b), effective area (c), and sensitivity (d) as a function of the energy of configuration **E1** compared to the reference configuration. This analysis uses a fixed data rate trigger.

4.4.2 25 tank trigger E1 vs A1

Discussion: The effect of the lower trigger threshold is plainly apparent in the effective area (panel c), which for this trigger shows the E-tank having superior low-energy collection area, whereas before it was an order of magnitude different lower. The E-tank appears to have slightly superior angular resolution, but poorer background rejection. It should be noted that the background rejection was seen to depend on the number of stations, and accordingly to section 6.4.1, the balance between the number of stations for A1 and E1 should vary -17% and +15%, respectively.

The sensitivity of **E1** in the low energy regime with this reduced trigger threshold is nearly identical to that of configuration **A1**.

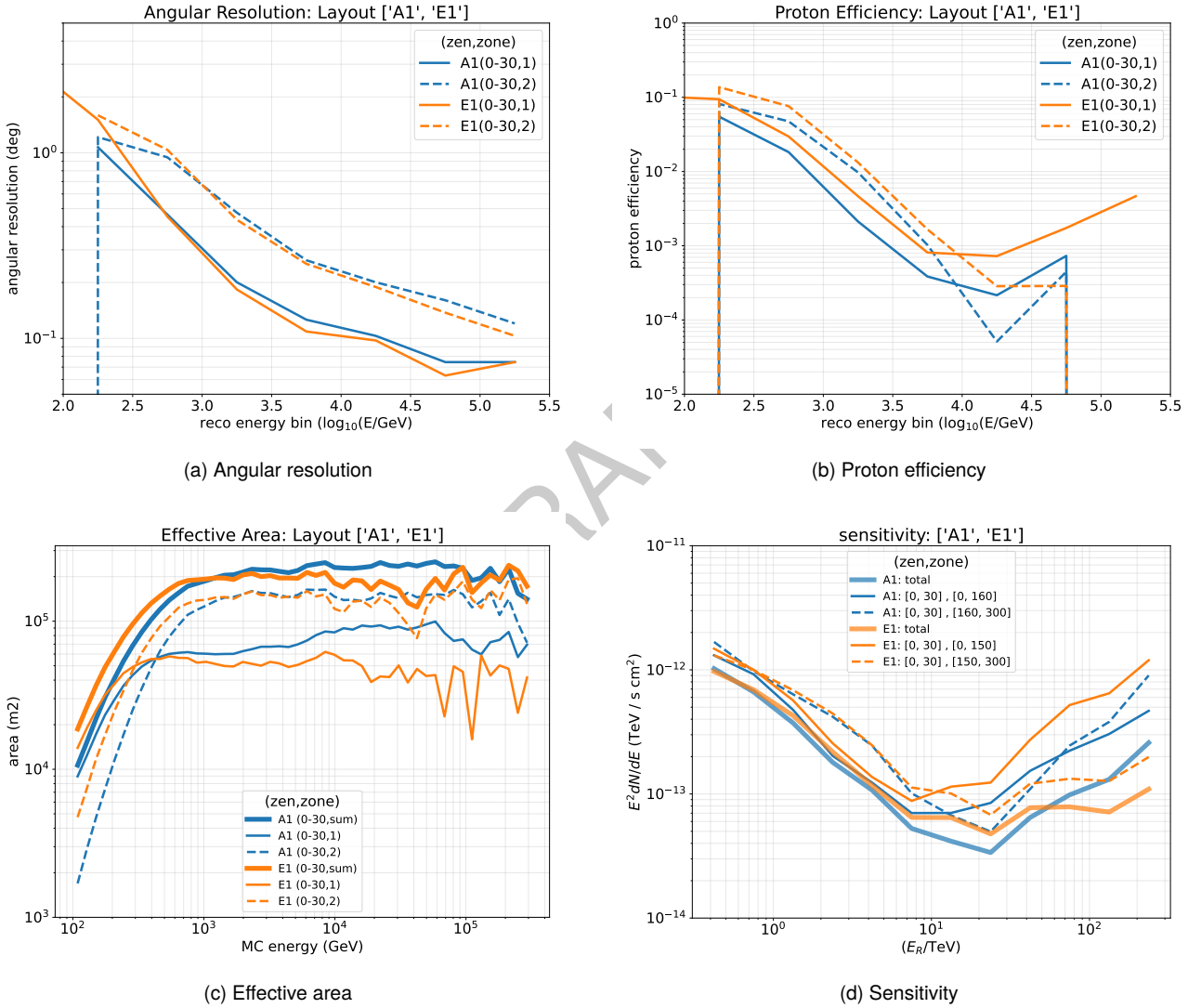

(a) Angular resolution

(b) Proton efficiency

(c) Effective area

(d) Sensitivity

Fig. 8 Angular resolution (a) proton efficiency (b), effective area (c), and sensitivity (d) as a function of the energy of configuration **E1** compared to the reference configuration **with a fixed minimum number of detector units in the (noise free) event of 25.**

4.5 F1: Reference layout with large 1-layer detector units

Motivation: This single-layer design is similar to the LHAASO and HAWC designs. The deeper upward-looking single PMT will have large muon signals (long path length) and is sufficiently deep that EM energy will range out far from the PMT to not mimic muon-like signatures. The cost per unit area is lower due to the less complex tank design and the absence of the second PMT.

Evaluation: Compare to **D1**, the large double layer tank. Pay special attention to the difference in the efficacy of the background rejection with the absence of the second layer.

Discussion: The Double-layer tank (D) shows slightly improved angular resolution compared to the single-layer tank (F) at high energy, probably due to the shallower upward-facing PMT. Unsurprisingly, the gamma-hadron separation in the double layer tank is improved compared to the single-layer with the additional muon-detector below. The single-layer tank only delivers a slightly higher effective area. Overall, the double-layer D-tank is equal or superior at all energies in our tests.

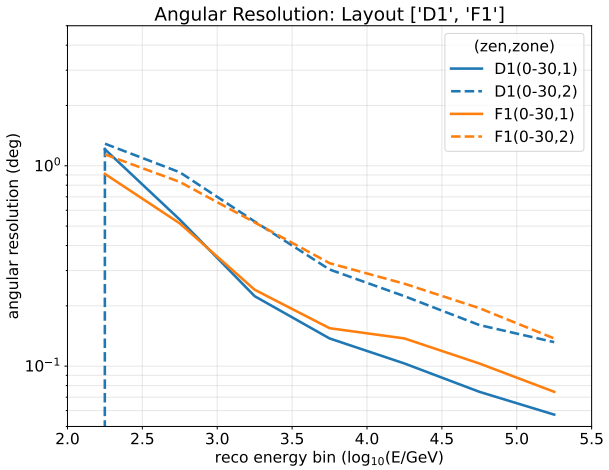

(a) Angular resolution

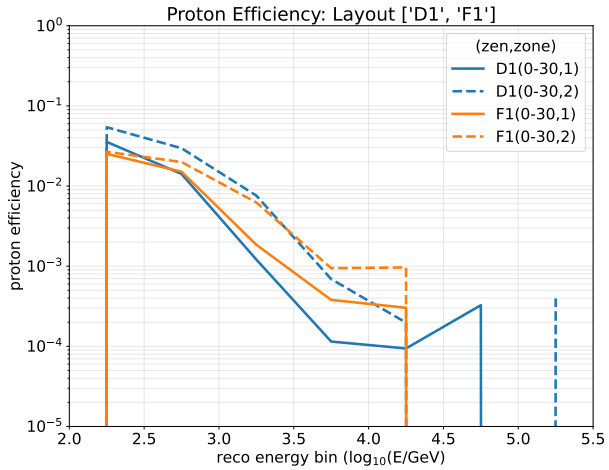

(b) Proton efficiency

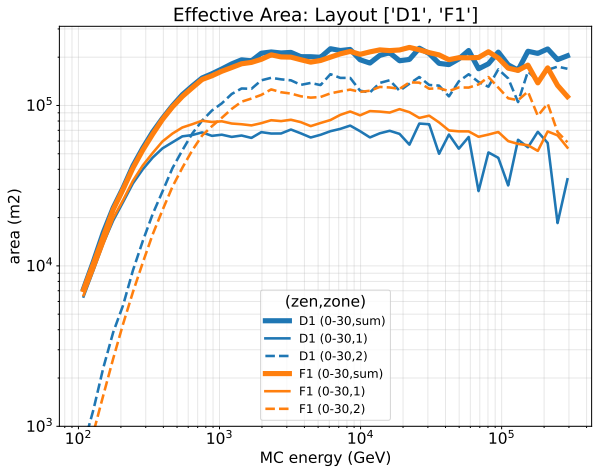

(c) Effective area

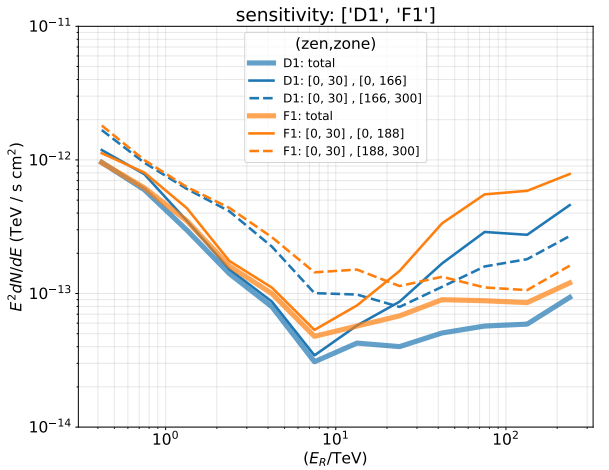

(d) Sensitivity

Fig. 9 Angular resolution (a) proton efficiency (b), effective area (c), and sensitivity (d) as a function of the energy of configuration **F1** compared to the configuration **D1** that features the same tank size but two layers.

5 Evaluation of the array layout configurations

In this section, we compare the 7 different array layouts. We perform this comparison using the A-tank as a standard reference. We also show the performance for sparse layout 4 with the E-tank, configuration **E4**, since the E-tank has a unique hadron rejection capability that may perform differently in an outer array.

5.1 A2: Reference tanks with 4 times larger coverage.

Motivation: In the layout, we wish to examine what happens if we generate a large constant density outer array (zone 2 radius 600 m), expanding the total detector footprint by 4×, to about the size of LHAASO KM2A. We achieve this expansion by reducing the size of zone 1 from R=160m to R=138m and reducing the fill factor of zone 2 from 5% to 2%.

Evaluation: Compare to reference design impact of a smaller inner array and larger outer array on low- and high-energy sensitivity, respectively.

Discussion: At low energy (below ∼1 TeV) the performance of A1 seems to be better in all parameters. Above ∼30 TeV, the large effective area of A2 start to significantly help for the sensitivity. Note, this happens at significantly higher energy than where A2 reaches full efficiency of the outer array, which is mostly a consequence of worse background rejection and angular resolution of the A2 configuration in the mid energy regime. The outer zone of A1 is still relativity close to the inner zone, which helps with the background rejection.

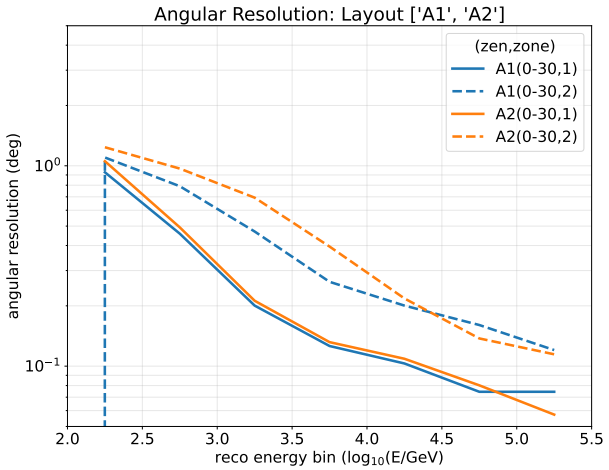

(a) Angular resolution

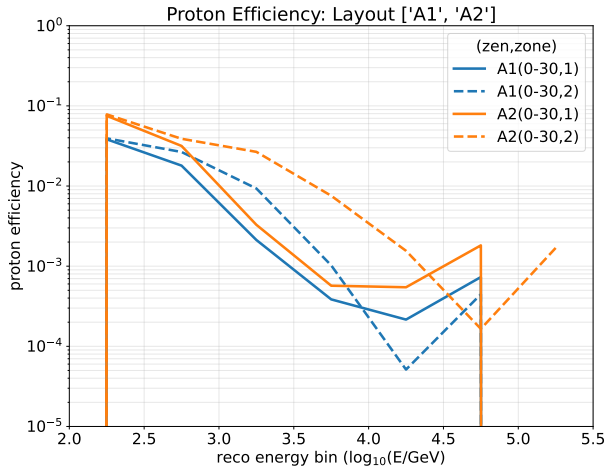

(b) Proton efficiency

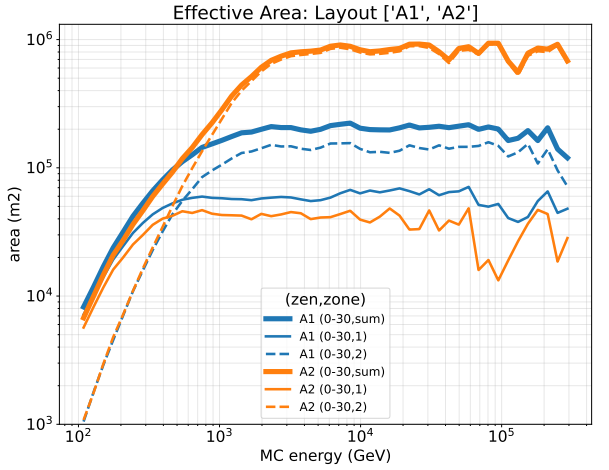

(c) Effective area

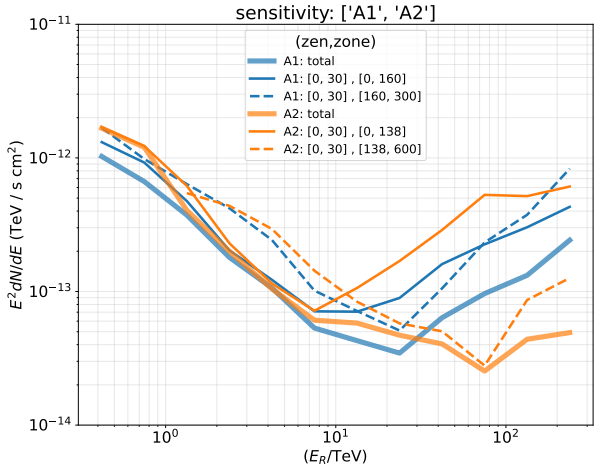

(d) Sensitivity

Fig. 10 Angular resolution (a) proton efficiency (b), effective area (c), and sensitivity (d) as a function of the energy of configuration **A2** compared to the reference layout **A1**.

5.2 A3: Reference Tanks with 4 times larger outer array radius with tanks in clusters.

Motivation: In this layout, we wish to study if clustering of A-type units in the outer array is beneficial compared to design **A3** for gamma-hadron separation. In addition, clustering might improve ease of deployment, network, and electronics layouts.

Evaluation: Study impact on performance of clustering with respect to **A2**. Comparison of gamma-hadron separation power and shower geometric reconstruction resolution.

Discussion: The performance of A2 and A3 are almost identical. The clustering of detector units is not significantly improving the gamma-hadron separation, neither seems it to degrade to other performance parameters.

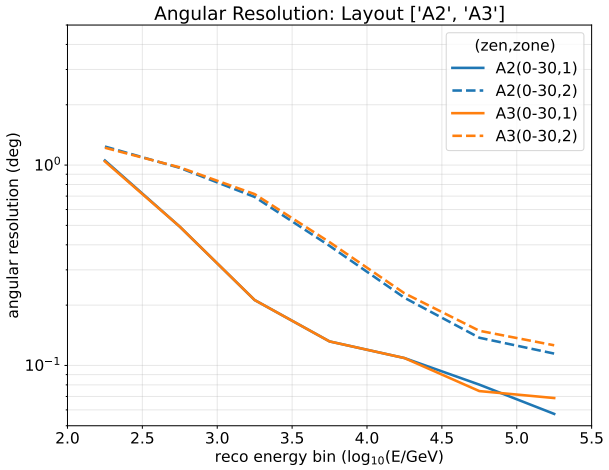

(a) Angular resolution

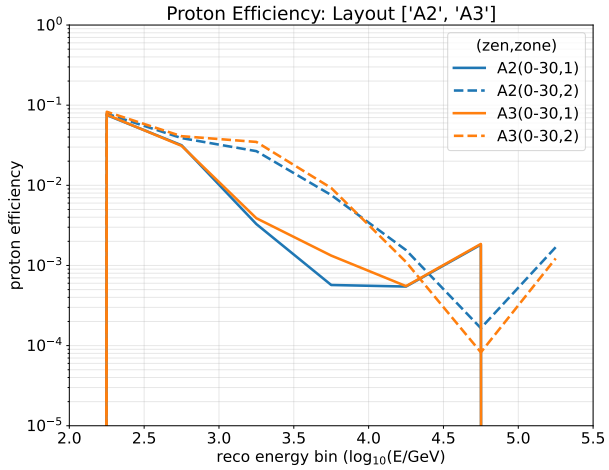

(b) Proton efficiency

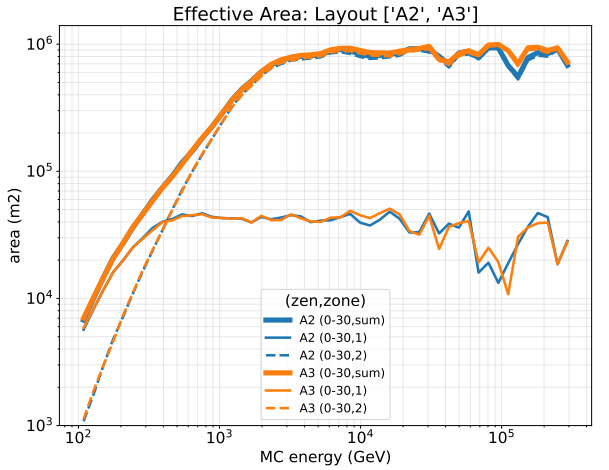

(c) Effective area

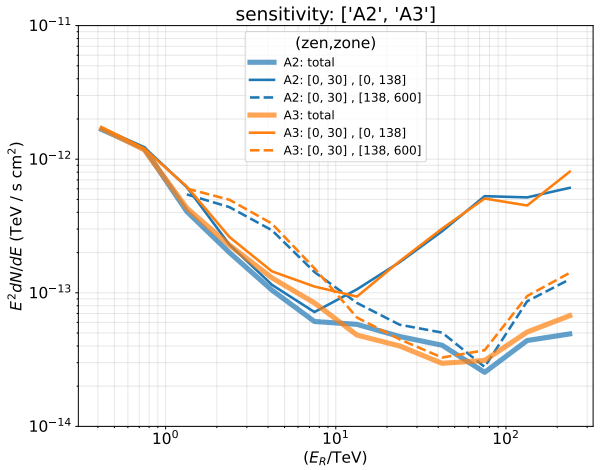

(d) Sensitivity

Fig. 11 Angular resolution (a) proton efficiency (b), effective area (c), and sensitivity (d) as a function of the energy of configuration **A3** compared to the reference layout **A1**.

5.3 A4: 3-zone graded array reference design

Motivation: An array layout with three zones might be a better fit for performance at different energy scales than two-zone models. This layout is similar to **A2**, with a similar size high-FF central zone, but the single 2.5% FF zone 2 covering the whole range R=[138m,600m] has been replaced with a combination of a 4% FF zone 2 with the range R=[140m,400m] and a third zone with a 1.25% FF covering R=[400m,600m]

Evaluation: The performance of this array will be compared to **A2**, which has similar parameters, but only two zones. Compare in detail performance as a function of energy compared to **A2**.

Discussion: It is hard to compare the zones directly for angular resolution, proton rejection and effective area, since the simulated zones are different in number and dimension. The overall sensitivity curve does show improvement in the low and mid-energy range ∼10 TeV, as we would expect from the introduction of the mid-FF zone, but seems to be slightly worse at the highest energies, since the region R=[400,600], has a higher FF for A2. We conclude that the graded approach, with more zones, is likely superior for coverage of a wide energy regime, where the FF of each zone is adjusted to optimize the scientific performance.

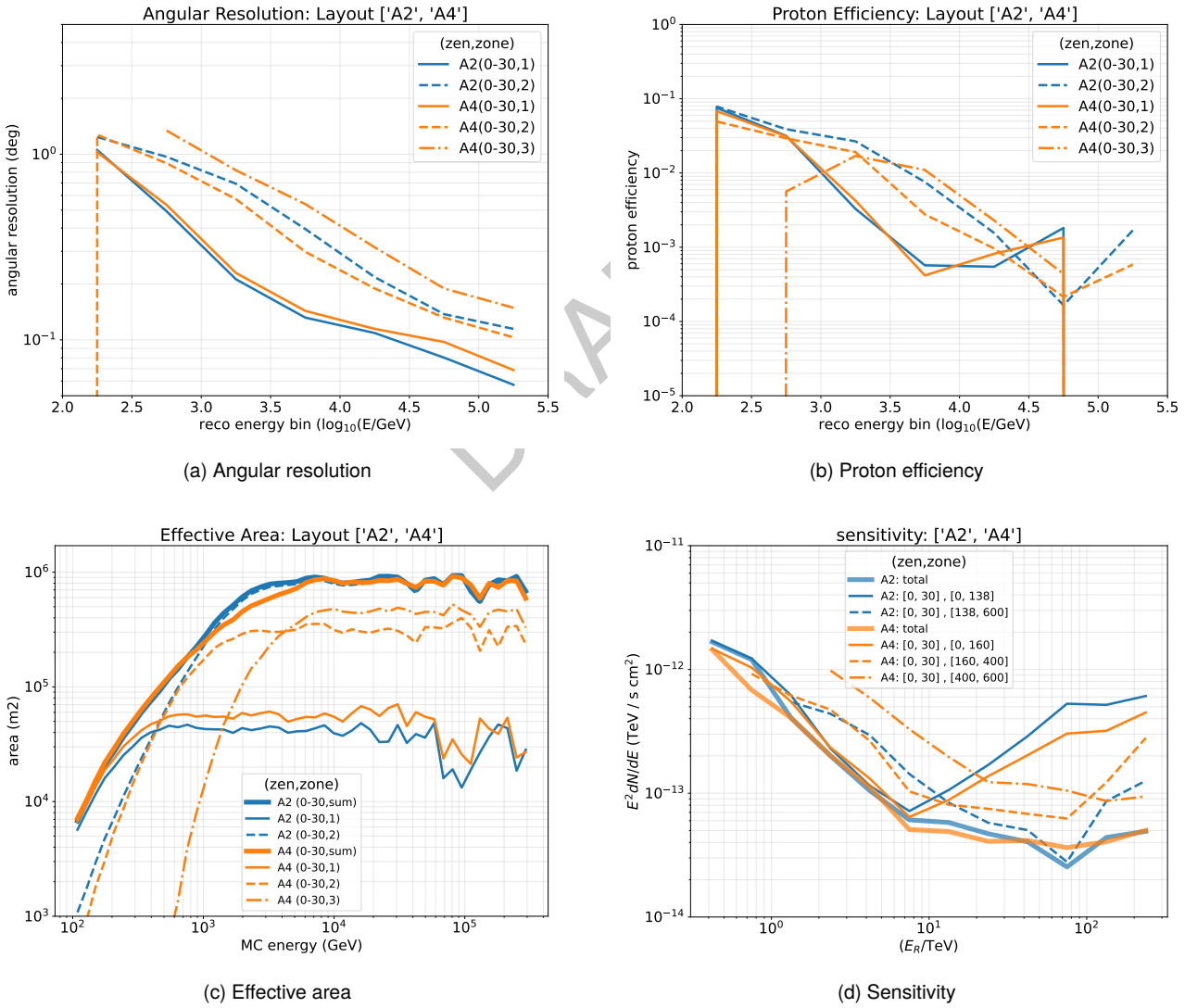

(a) Angular resolution

(b) Proton efficiency

(c) Effective area

(d) Sensitivity

Fig. 12 Angular resolution (a) proton efficiency (b), effective area (c), and sensitivity (d) as a function of the energy of configuration **A4** compared to the reference layout **A1**.

5.4 A5: Lower density inner array

Motivation: Increasing the size of the inner array at the cost of a lower fill factor might impact the reconstruction and classification of events positively, as more showers will be better contained in the inner array. Configuration **A5** has a zone 1 FF or 40%, compared to 80% for the reference configuration **A1**. However, the lower FF may compromise the inner array's reconstruction performance.

Evaluation: Compare with layout **A1**. Evaluate the impact on the shower geometric reconstruction and gamma-hadron separation in the energy regime $\sim$ 10 TeV.

Discussion: We find that the low-FF array is not superior to the reference layout (**A1**) in any energy regime, with the possible exception of the range above $\sim$ 50 TeV. In the high-energy regime, however, greater improvement in the high-energy regimes is achieved by layouts 2,3 and 4. It is interesting, considering the drastic reduction in FF, that the low-energy performance is not compromised compared to the reference.

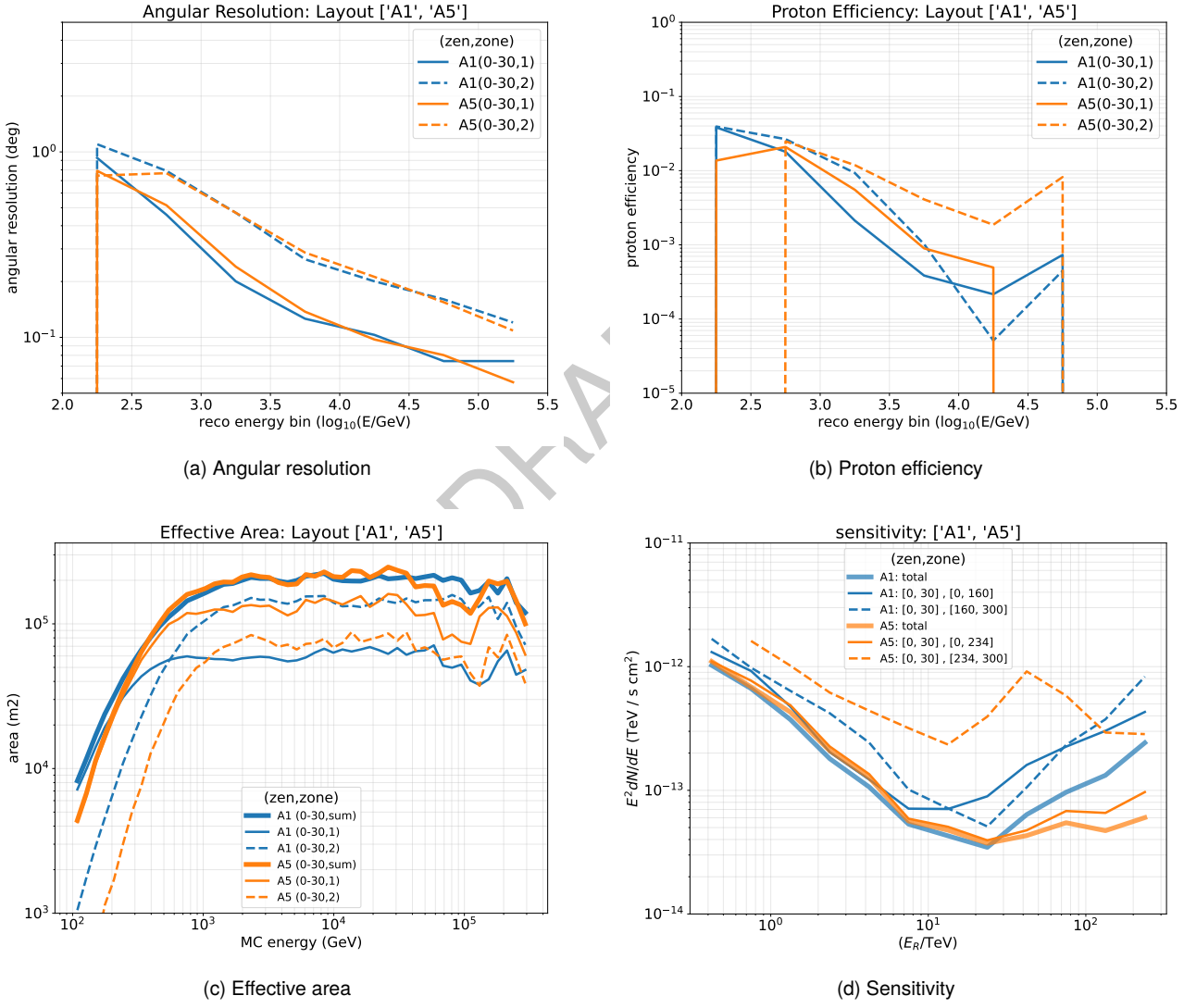

(a) Angular resolution

(b) Proton efficiency

(c) Effective area

(d) Sensitivity

Fig. 13 Angular resolution (a) proton efficiency (b), effective area (c), and sensitivity (d) as a function of the energy of configuration **A5** compared to the reference layout **A1**.

5.5 A6: Ultra-compact array

Motivation: Test what impact is of a maximally-dense inner array with only a small outer array. Layout 6 has a density of fill factor = 88% compared to 80% for the central zone and a reduced FF for zone 2 to maintain equal zone 1 area. Note, 88% fill factor is the maximum for close packed cylinders.

Evaluation: How will a maximally dense inner array impact the lower energy performance with respect to the reference layout **A1**?

Discussion: Only slightly improved low-energy performance is observed. At no energy is the ultra high FF seen to be significantly beneficial. Note that improving the overall FF by 10% will not improve the shower particle detection rate by that same factor, since for even slightly of zenith angles, the spaces between tanks are shadowed by the neighboring tanks.

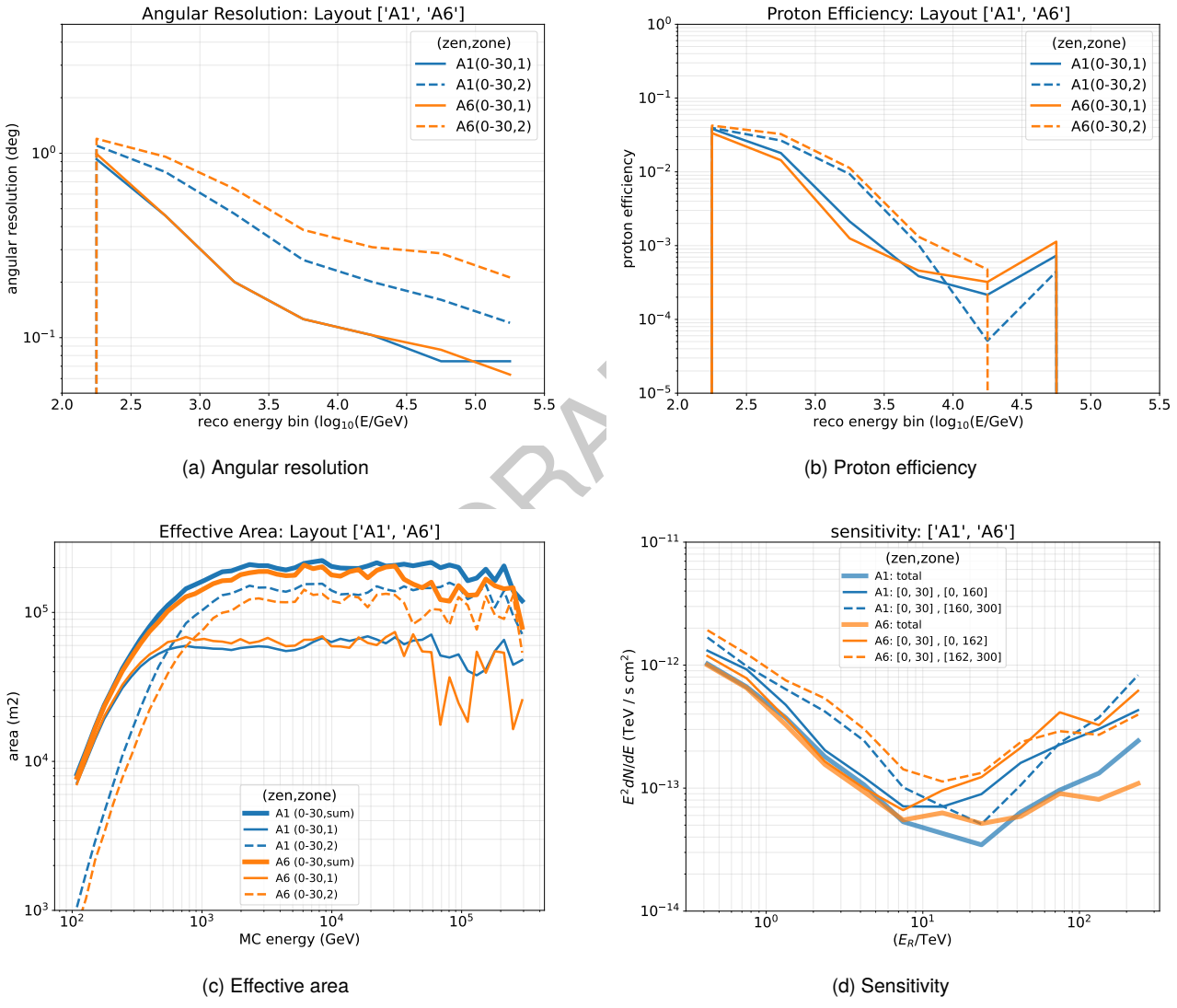

(a) Angular resolution

(b) Proton efficiency

(c) Effective area

(d) Sensitivity

Fig. 14 Angular resolution (a) proton efficiency (b), effective area (c), and sensitivity (d) as a function of the energy of configuration **A6** compared to the reference layout **A1**.

5.6 A7: 3-zone extremely large array

Motivation: At the cost of less investment in the inner array and an extremely low FF how much can we push the high energy regime? In this test, we consider a 3-zone detector with a coverage of more than $4km^2$. We are only able to cover this area by reducing the fill factor to 0.63% and substantially reducing the size of the central zone. It is not clear whether an array with such an extremely low FF will be able to reliably reconstruct showers and efficiently reject backgrounds. For comparison, the LHAASO KM2A muon detectors have a FF Array Trigger$\times$ higher than we simulate here, about 5-6%.

Evaluation: Test loss of performance at low energy vs gain at higher energy. Test feasibility of large low-density zone for the outer array.

Discussion: As expected, the low-energy and medium-energy performance is much worse for the extremely large array, but above 30 TeV, the larger area leads to a significantly improved sensitivity for the larger array. However, note that the sensitivity at these high energies comes entirely from zone 2, which has a FF of 2.5%. We conclude that extremely low FFs are not effective in the regime from 30-300 TeV. Layout 2 or layout 4 is superior for extension of the total high-energy area without compromising the low-energy performance.

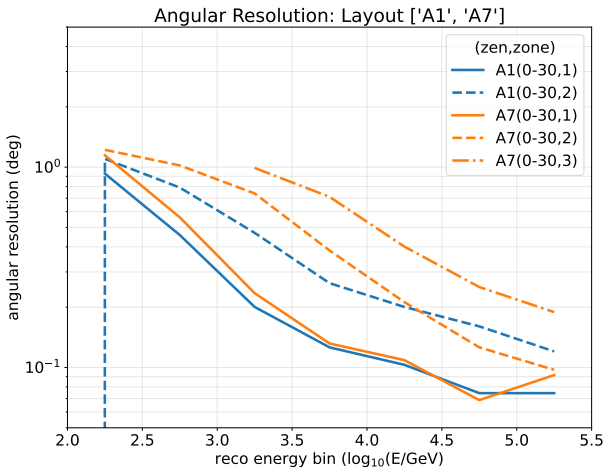

(a) Angular resolution

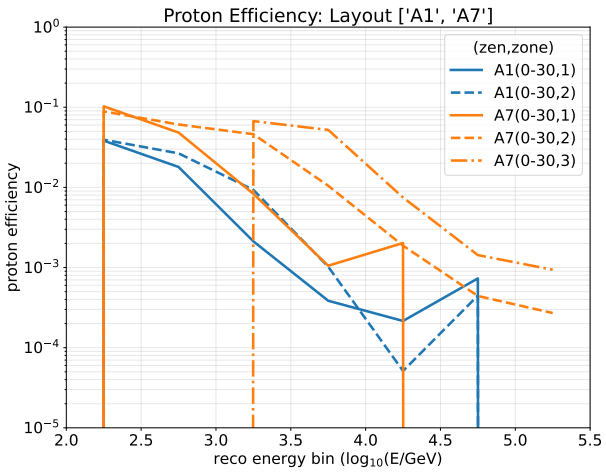

(b) Proton efficiency

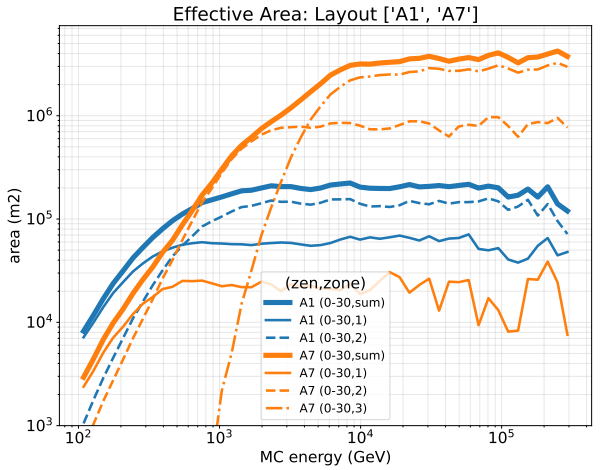

(c) Effective area

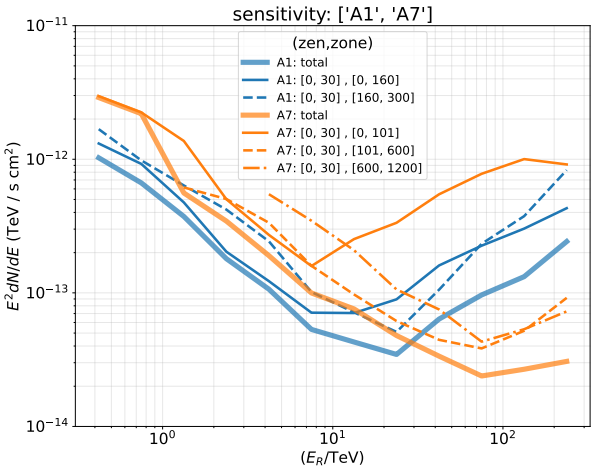

(d) Sensitivity

Fig. 15 Angular resolution (a) proton efficiency (b), effective area (c), and sensitivity (d) as a function of the energy for configuration **A7** compared to the reference layout.

5.7 E4: Mercedes station with graded array

Motivation: Assess the performance of the *Mercedes* station in a graded 3-zone array. The main motivation is the performance of the gamma-hadron discriminator for different shower energy scales.

Evaluation: The performance of configuration **E4** should be directly comparable with layout **A4**.

Discussion: We note that the outer zone gamma-hadron separation performance does not significantly differ from what was shown with the **A1-E1** comparison.

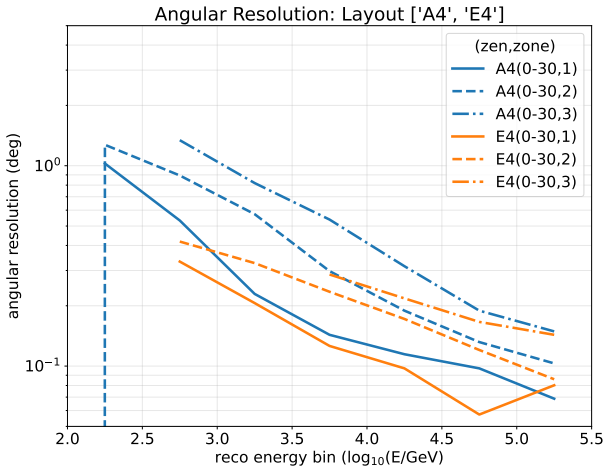

(a) Angular resolution

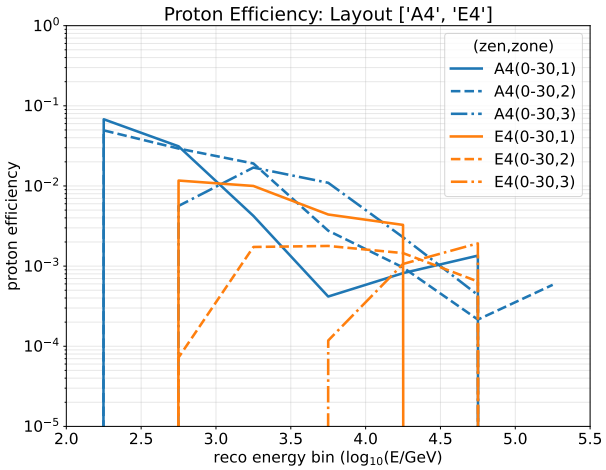

(b) Proton efficiency

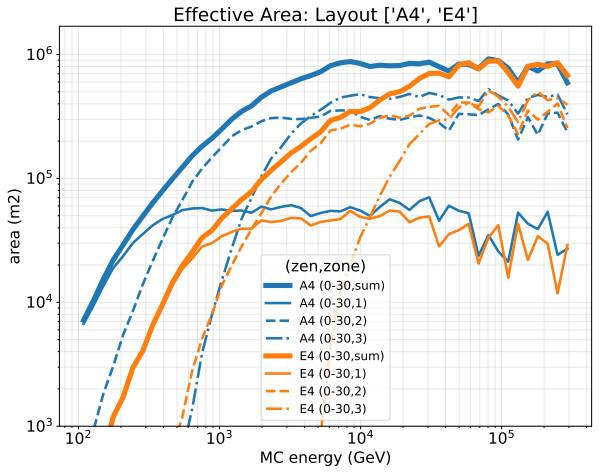

(c) Effective area

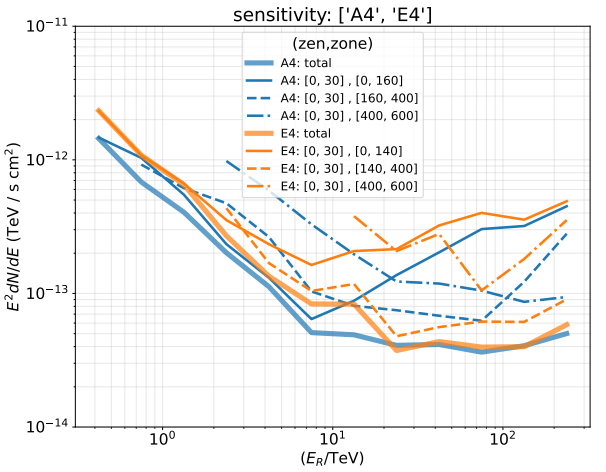

(d) Sensitivity

Fig. 16 Angular resolution (a) proton efficiency (b), effective area (c), and sensitivity (d) as a function of the energy of configuration **E4** (Mercedes design) compared to the reference station with the same array layout (**A4**).

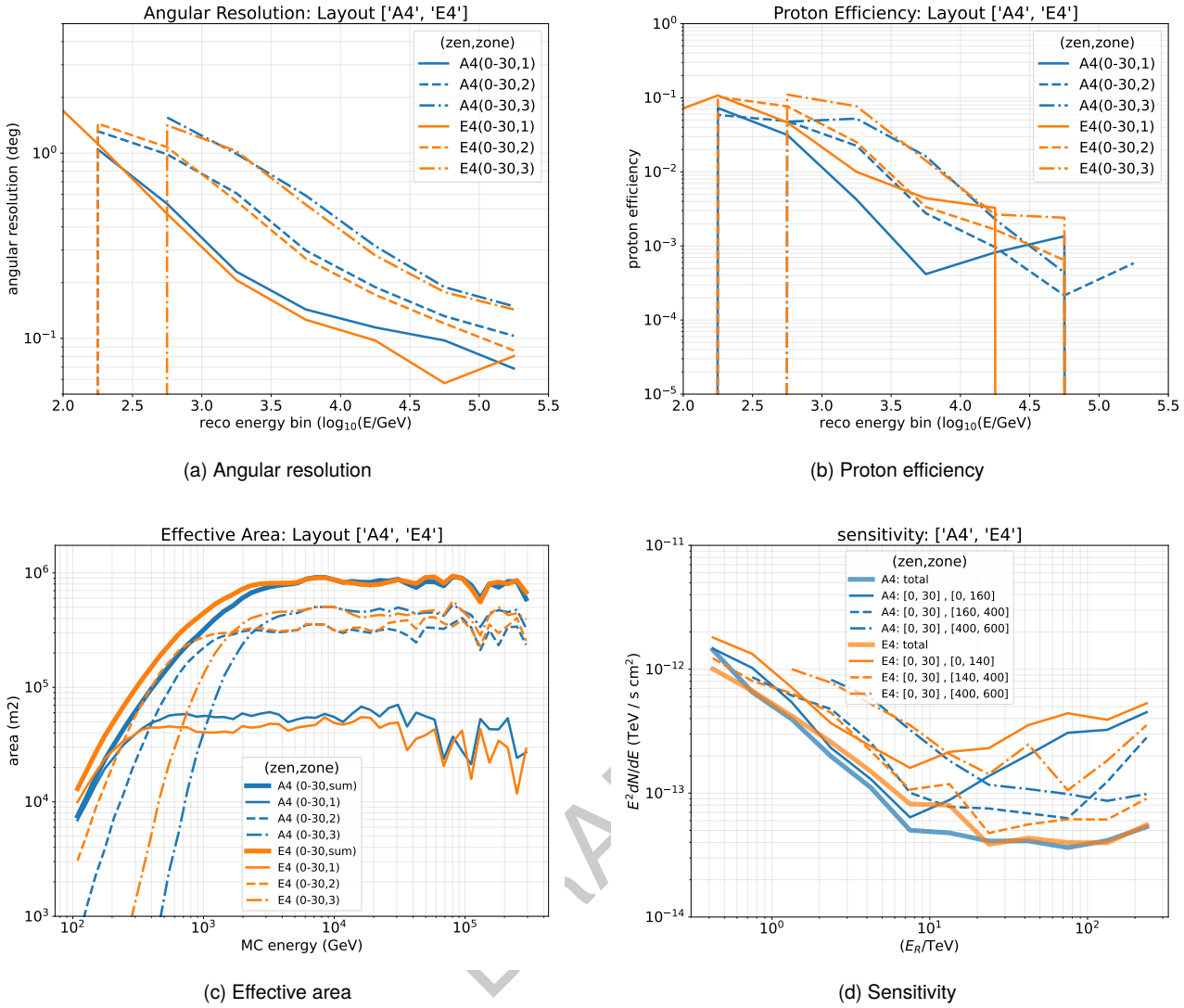

(a) Angular resolution

(b) Proton efficiency

(c) Effective area

(d) Sensitivity

Fig. 17 Angular resolution (a) proton efficiency (b), effective area (c), and sensitivity (d) as a function of the energy of configuration **E4** (Mercedes design) compared to the reference station with the same array layout (**A4**),**with a fixed minimum number of detector units in the (noise free) event of 25.**.

6 General Considerations and Discussion

In the previous sections we addressed basically the questions for which the individual configurations were designed. In this section we will try to capture the overall behaviour of the different configuration and address issues that were not fully addressed by in the previous sections.

6.1 Energy Resolution

Energy resolution and bias has not been shown in the previous sections, as it does not impact the source detection sensitivity, but is important for certain science cases. Therefore we show in Figure 18 and 19 for respectively the different units and layouts.

In general the conclusion can be drawn that energy resolution and bias are quite similar for the different detector station designs and layouts. With the notable exception of the outer array of A7 (zone 3). Indicating that the 0.62 % fill factor impacts these parameters significantly.

The fact that the energy resolution does not vary from detector to detector is likely a result of the fact that the

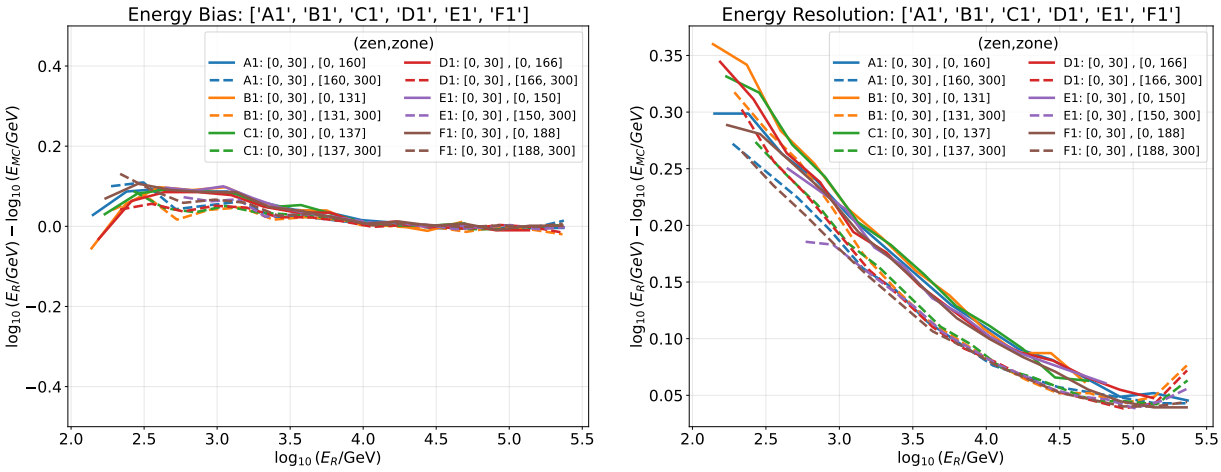

Fig. 18 Energy bias (left) and resolution (right) for different detector-unit designs.

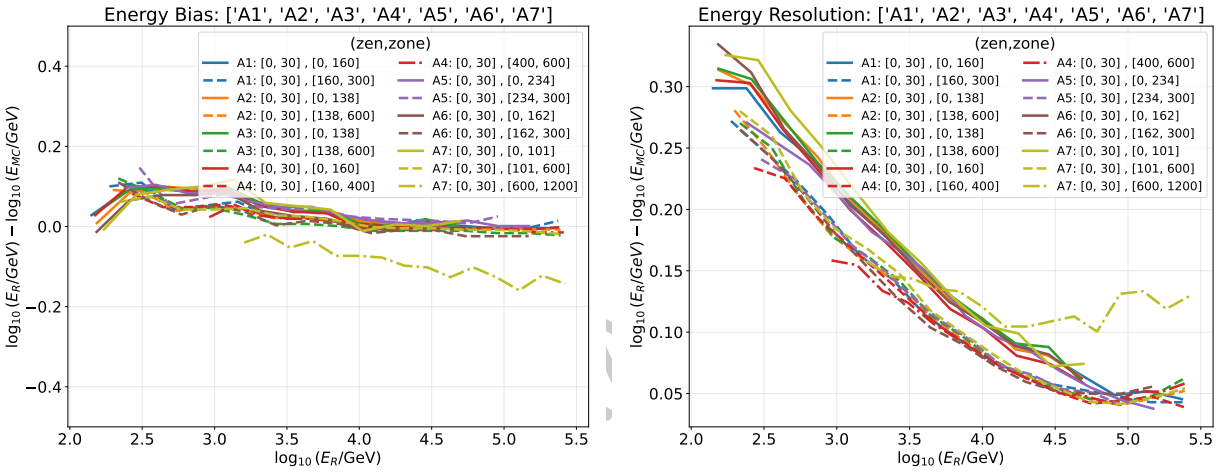

Fig. 19 Energy bias (left) and resolution (right) for different array layouts.

main source of energy error is the fluctuation of the depth of the first interaction depth of the primary gamma-ray in the atmosphere, which is independent of the detector type or layout.

6.2 Shower Inclination Dependence

We show most performance figures (except sensitivity) only for low zenith angles (below 30 degrees). In Figure 20 we show for zone 2 for the A1, E1, and F1 configurations the proton efficiency in two different zenith angle ranges. These tanks have different physical sizes and PMT configurations, which might impact the proton efficiency differently for different zenith angles. However, this figure shows no clear indication for a drastic change with zenith angle, which might be partly caused by low statistics at the high energy regime where a potential effect could occur.

6.3 Black versus white walls

A production of `swgo-reco` has been made with poorly reflecting walls (10% reflection coefficient) for the configurations A1, C1, D1, and F1. Unfortunately, we have not completed the retraining of the machine-learning algorithms on these set before the deadline of the milestone. However, a study has been performed on the array trigger rates on a subset of the configurations and the results are presented in table 4.

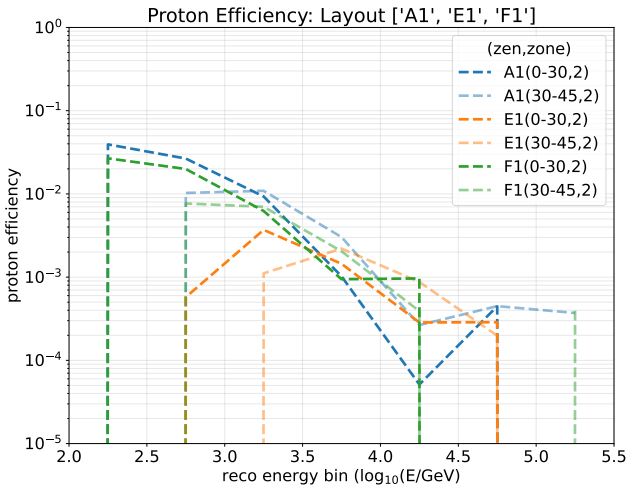

Fig. 20 Impact of the shower zenith angle on the proton efficiency as a function of the energy in the different studied detector concepts A1,E1, and F1. These are shown for zone 2.

Configuration	Threshold T	Average $\langle M_{128} \rangle$
A1	29	19
B1	23	16
C1	22	17
D1	25	17

Tab. 4 Array Trigger settings poorly reflecting walls in the upper chamber with variables (same as table 3)

From this we conclude that the multiplicity triggers are significantly lower than in the case of the reflective walls table 3. This might have significant impact on the resulting performance figures, we therefore suggest to still estimate the performance of the black-walled double layer designs.

6.4 Detector Costing and Scaling Models

Since the configurations to be simulated were frozen with the M5 milestone, the Detector Group has updated costs for the various detector designs. We will approximate the improvement in sensitivity associated with the changes in cost in this section using a generalized scaling model derived from simulations.

6.4.1 Detector Configurations

Label	Unit Cost in Past[6] (USD)	Unit Cost in Present[7] (USD)	Variation (%)
A	9680	11335	+17
B	10662	11682	+10
C	6901	10284	+49
D	14321	15368	+7
E	11882	10122	-15
F	11538	13689	+19

Tab. 5 Updated cost estimates for the detector unit designs used in the M6 exercise (costs revised as of 2024-03-25).

SECTION TO BE COMPLETED

Use the results obtained from configurations **A5** (Lower density) and **A6** (Ultra compact) to evaluate the effects of altering the number of stations in the compact array in response to changes in the cost of the detector station,

as outlined in table 5.

6.4.2 Array Layout Configurations

The conclusions regarding the array layouts are based on the detector implemented in the **A1** configuration, with the exception of **E4**. Therefore, any variations in the cost of the detector are not expected to impact the overall findings significantly.

6.5 Sensitivity curves

For the convenience of the reader, here we combine the sensitivity curves for the 6 station type and 7 configurations on simple figures. Figure 21 shows the 6 sensitivity curves for the station types **A1-F1**. The accompanying figure shows the same data plotted w.r.t. configuration **A1**. Figure 22 shows the sensivity curve for the 7 simulated layouts using the A tank as a standard reference station. As before, the second figure shows the relative sensivitiy compared to **A1**.

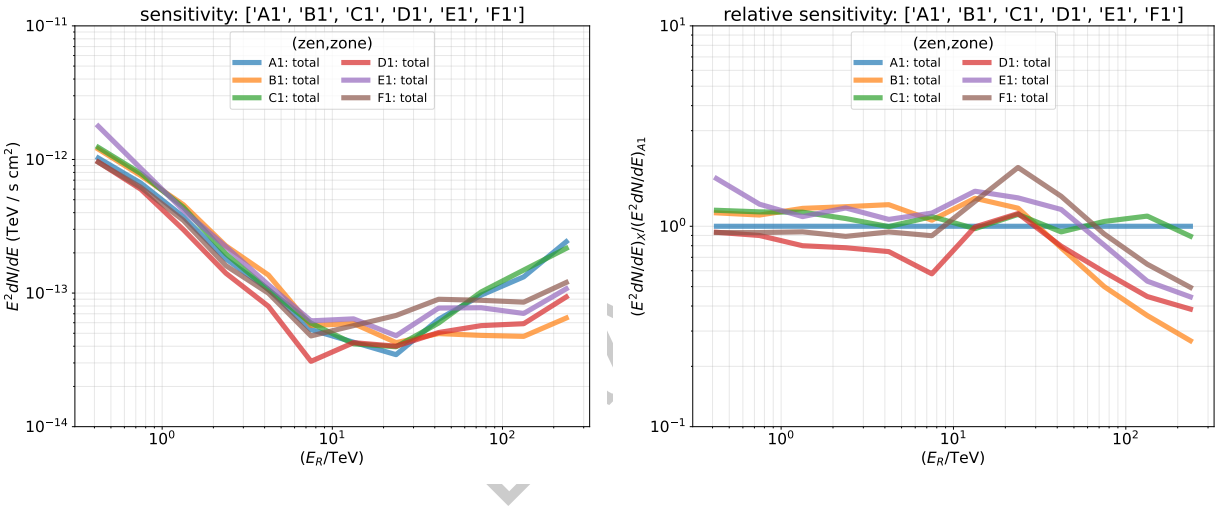

Fig. 21 Left: Differential point source sensitivity as a function of reconstructed energy shown for the studied detector-unit designs. Right: Relative sensitivity to A1 configuration.

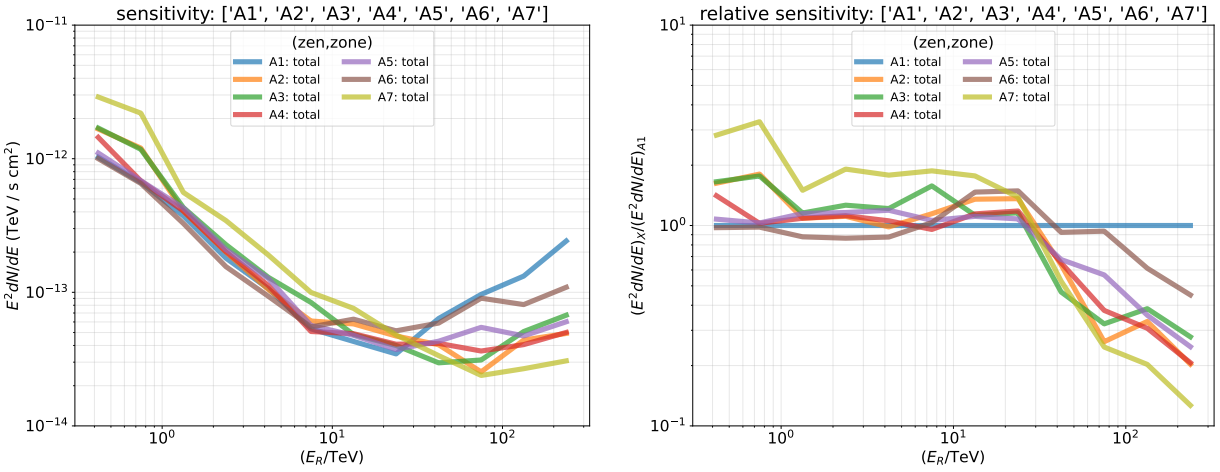

Fig. 22 Left:Differential point source sensitivity as a function of reconstructed energy shown for the studied array layouts. Right: Relative sensitivity to A1 configuration.

7 Final Remarks

TO BE COMPLETED Summary of main findings and open issues which should be addressed in Milestone 7.

References

[1] R. Conceição et al. *Detector unit and array configurations for M5 (v3)*. 2022. URL: https://www.swgo.org/SWGOWiki/lib/exe/fetch.php?media=simulations:swgo_m5_configurations-v3.pdf.

[2] S. Kunwar et al. 'A double-layered Water Cherenkov Detector array for Gamma-ray astronomy'. In: *Nuclear Instruments and Methods in Physics Research Section A: Accelerators, Spectrometers, Detectors and Associated Equipment* 1050 (2023), p. 168138. ISSN: 0168-9002. DOI: https://doi.org/10.1016/j.nima.2023.168138. URL: https://www.sciencedirect.com/science/article/pii/S0168900223001286.

[3] H. Schoorlemmer et al. *Documentation on the production of the Instrument Response Functions (v0.1)*. 2024. URL: https://www.swgo.org/SWGOWiki/lib/exe/fetch.php?media=simulations:swgo-as-24-002v0.1.pdf.

[4] J. Hinton. *R&D Phase Plan v1.6*. July 2023. URL: https://www.swgo.org/SWGOWiki/lib/exe/fetch.php?media=swgoplan1.6.pdf.

Appendix A

7.1 Shower geometry reconstruction

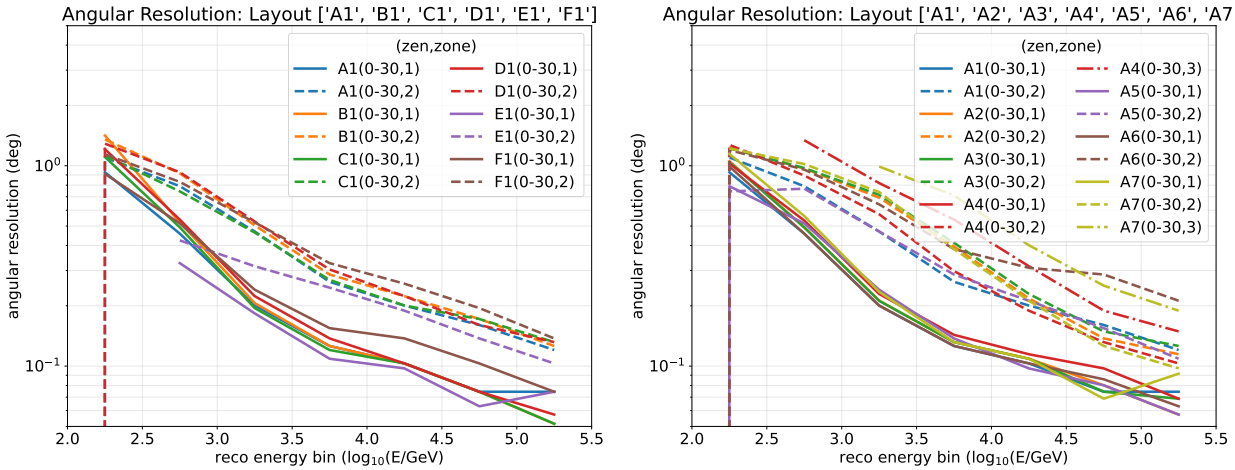

Fig. 23 Angular resolution as a function of the energy for air showers with zenith angles below 30 degrees. Left: detector units. Right: layouts.

7.2 Gamma/hadron discrimination

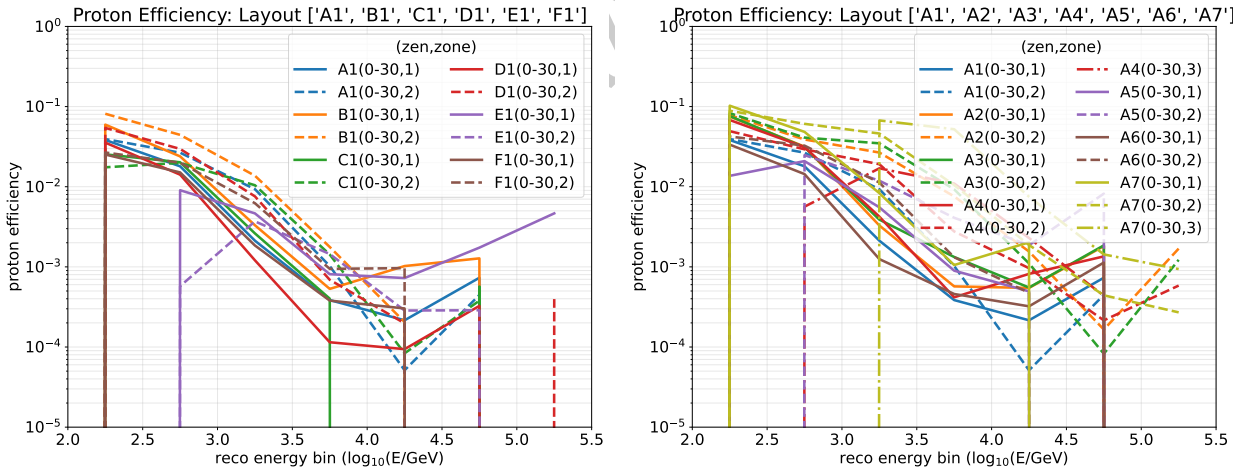

Fig. 24 Proton efficiency as a function of the energy shown for air showers with zenith angles between 0 - 30 degrees. Left: detector units. Right: layouts.